BIRZEIT UNIVERSITY

Faculty of Engineering and Technology

Master in Computing

Photovoltaic Integration in a Grid Power System

النظام الكهروضوئي المدمج بالشبكة الكهربائية

By

Noureddin Motan

Supervisor

Dr. Muhammad Abu-Khaizaran

This thesis is submitted in partial fulfillment of the requirements for the Master's Degree in Computing from the Faculty of Engineering and Technology at Birzeit University, Palestine

Committee

Dr. Muhammad Abu-Khaizaran

Dr. Basim Alsayid

Dr. Jaser Sa'ed

November 22, 2017

Faculty of Engineering and Technology

Master in Computing

Photovoltaic Integration in a Grid Power System

النظام الكهروضوئي المدمج بالشبكة الكهربائية

By

Noureddin Motan

Supervisor

Dr. Muhammad Abu-Khaizaran

Committee	Signature
Dr. Muhammad Abu-Khaizaran	……………………………
Dr. Basim Alsayid	……………………………
Dr. Jaser Sa'ed	……………………………

November 22, 2017

Acknowledgement

I would first like to express my gratitude to my supervisor, Dr. Muhammad Abu-Khaizaran, who never hesitated to provide support and guidance by sharing his knowledge and creative ideas. All that helped me to achieve my goals and complete the thesis successfully.

I would also like to thank the discussion committee, Dr. Basim Alsayid and Dr. Jaser Sa'ed, for their valuable comments, suggestions and precious time to review the thesis.

Finally, I would like to acknowledge with appreciation the patience and support from my family, especially my parents and my wife, who encouraged me to take the first step to the master program and always been there throughout the whole period of my study.

Abstract

Grid-connected Photovoltaic (PV) systems have increased dramatically in the last few years due to the increased global interest in renewable energy sources and the growth in energy demand. As a consequence, new and modern control strategies should be applied to improve the efficiency, reliability, and stability of grid-connected PV systems. To achieve that, the whole PV system should be tested under various weather and grid conditions. However, the wide variety of the PV system devices and control algorithms, in addition to the destructive nature of many types of scenarios and faults, make the practical testing of the PV system very difficult, very expensive, and impossible in many cases. Therefore, this thesis made use of the modelling and simulation tools of MATLAB/SIMULINK to develop a model for a grid-connected PV system.

The developed model implements all components of the grid-connected PV system; these components are a PV array, boost converter, Maximum Power Point Tracking (MPPT) controller, three-phase Voltage Source Inverter (VSI), grid filter, grid synchronization method and VSI controller. Each component of the system was modelled, tested and validated. Then the whole PV system was used to simulate many scenarios under various grid and weather conditions. The simulation results show that the model is reliable, stable and suitable for studying the grid-connected PV system.

الملخص

لقد ازدادت النظم الكهروضوئية المتصلة بالشبكة الكهربائية بشكل كبير في السنوات القليلة الماضية بسبب تزايد الاهتمام العالمي بمصادر الطاقة المتجددة وزيادة الطلب على الطاقة. ونتيجة لذلك، ينبغي تطبيق استراتيجيات تحكم جديدة وحديثة لتحسين كفاءة وموثوقية واستقرار النظم الكهروضوئية المتصلة بالشبكة. ولتحقيق ذلك، يجب اختبار النظام في ظل ظروف الطقس والشبكة المختلفة والمتغيرة. ولكن وجود مجموعة واسعة من الاجهزة الكهربائية وخوارزميات التحكم المكونة للنظام، بالإضافة إلى الطبيعة المدمرة لأنواع كثيرة من السيناريوهات والأخطاء، يجعل الاختبارات العملية للنظام صعبة ومكلفة ومستحيلة في كثير من الحالات. ولذلك، فإن هذه الأطروحة تستخدم أدوات النمذجة والمحاكاة التي يوفرها برنامج "MATAB/SIMULINK" لبناء نموذج للنظام الكهروضوئي المتصل بالشبكة.

النموذج المبني يشمل جميع اجزاء نظام انتاج الطاقة الكهروضوئية المتصل بالشبكة؛ وهذه المكونات هي مصفوفة الألواح الكهروضوئية، رافع الجهد المستمر "Boost converter"، نظام التحكم المسؤول عن تتبع الحد الاقصى للطاقة الناتجة من مصفوفة الألواح الكهروضوئية"MPPT controller" ، عاكس الجهد ثلاثي الاطوار "VSI"، مرشح الشبكة"grid filter" ، نظام التحكم والمزامنة بين نظام الطاقة الكهروضوئية والشبكة الكهربائية العامة. في هذه الاطروحة تم نمذجة وبناء كل عنصر من مكونات النظام واختباره والتحقق منه. ثم تم استخدام كامل النظام الكهروضوئي المطور لمحاكاة العديد من السيناريوهات تحت ظروف الطقس والشبكة المختلفة والمتغيرة. وقد اظهرت نتائج المحاكاة أن النموذج المبني موثوق ومستقر ومناسب لدراسة النظام الكهروضوئي المتصل بالشبكة.

Table of Contents

List of Figures

List of Tables

List of Abbreviations

PV	Photovoltaic
CAGR	Compound Annual Growth Rate
MPPT	Maximum Power Point Tracking
EMI	Electromagnetic Interference
PLL	Phase Locked Loop
c-Si	crystalline Silicon
sc-Si	single crystalline Silicon
mc-Si	multi-crystalline Silicon
a-Si	Amorphous Silicon
μc-Si	microcrystalline Silicon
CdTe	Cadmium-Telluride
CIGS	Copper-Indium-Gallium-Diselenide
STC	Standard Test Condition
ISDM	Single Diode Model
SDM	The Single Diode Model
DDM	Double Diode Models
SSDM	Simplified Single Diode Model
IC	Incremental Conductance
P&O	Perturb and Observe
MPP	Maximum Power Point
PWM	Pulse Width Modulation
PI	Proportional Integral
PR	Proportional Resonant
VCO	Voltage-Controlled Oscillator
PCC	Point of Common Coupling
FB	Full-Bridge
NPC	Neutral Point Clamped
THD	Total Harmonic Distortion

Chapter 1   INTRODUCTION

1.1 Introduction and Motivation

Solar Photovoltaic (PV) system is a system that employs solar cells to convert solar energy into electrical power. The solar cell, or the PV cell, is an electrical device that produces electricity directly from the sunlight. Solar PV system is one of the renewable and clean energy sources.

The tremendous increase in energy demand, the growth of global interest in renewable and clean energy sources, and the advances in research and technology in solar PV, all led to significant advances in PV industry. For instance, the PV cost benchmark for residential PV systems in U.S. decreased from $7.06/Wdc in 2009 to $2.93/Wdc in 2016 (as shown in Figure 1-1) [1]. Moreover, as shown in Figure 1-2, PV energy production soared from below 10 GW in 2006 to more than 300GW in 2016 . In addition, During 2016, more than 75 GW of solar PV capacity was added worldwide, compared to 50 GW in 2015 [2]–[4]. According to [5] "the Compound Annual Growth Rate (CAGR) over the last 15 years was above 40 %, which makes PV one of the fastest growing industries at present".
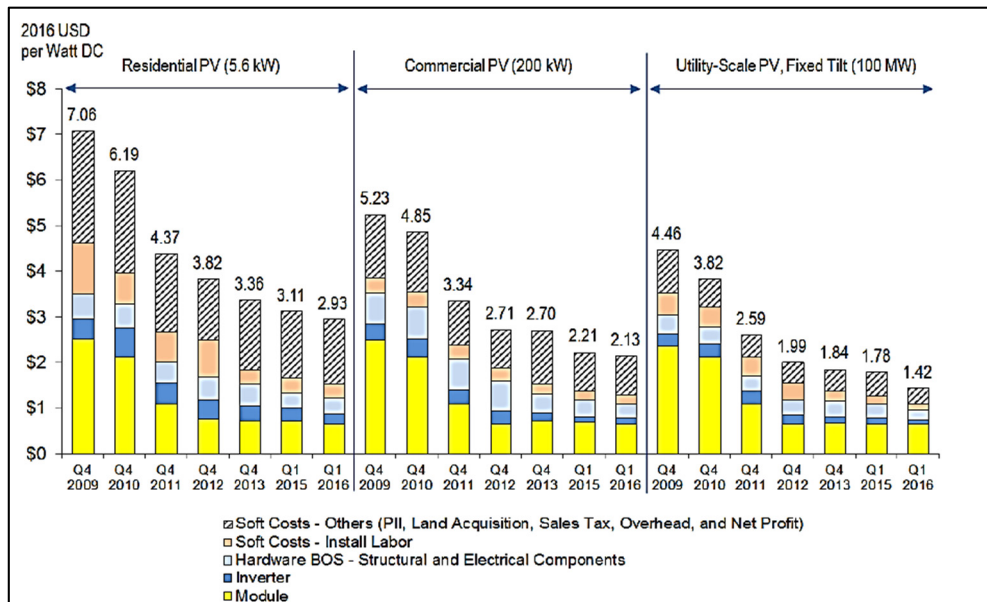
Figure 1-1 PV System Cost Benchmark Summary [1]
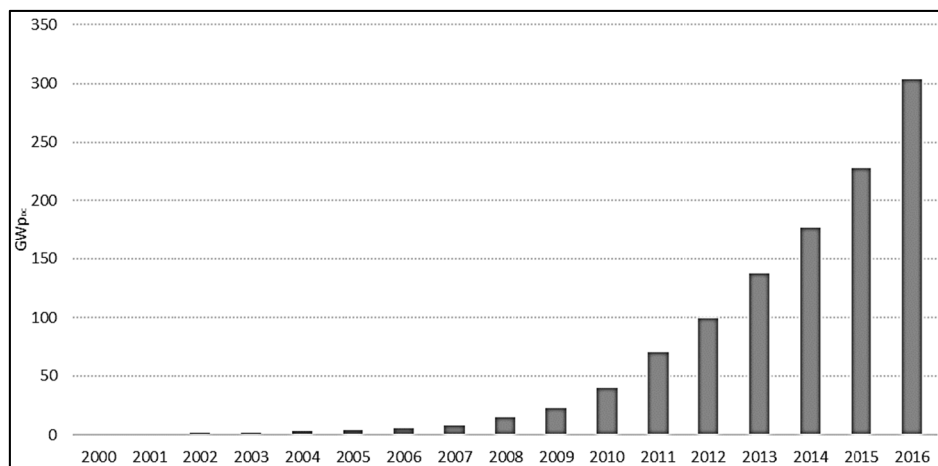
Figure 1-2 Evolution of PV Installation [2]

PV systems can be classified into two major classes: grid-connected PV systems and off-grid (stand-alone) PV systems. The grid-connected PV systems operate in parallel with electric grid to increase the output power of the grid, while off-grid systems have no connection to the electric grid. Off-grid systems are used in some applications such as roof-mounted PV system, solar vehicle, solar powered lamps, and water pumps [6]. Nowadays, the vast majority of PV systems are grid-connected, while off-grid applications represent only 1% of the market, down from more than 90% two decades ago [7].

As the importance of grid-connected PV systems, this thesis focuses on modelling and control of the grid-connected PV system, using MATLAB/SIMULINK, to achieve a high efficient, stable and reliable power system.

Figure 1-1 shows a typical grid-connected system. Typically, it consists of a PV array, a Maximum Power Point Tracking (MPPT) Controller, a DC-DC converter, a DC-AC inverter, grid interface, control unit, and protection interfacing [6].
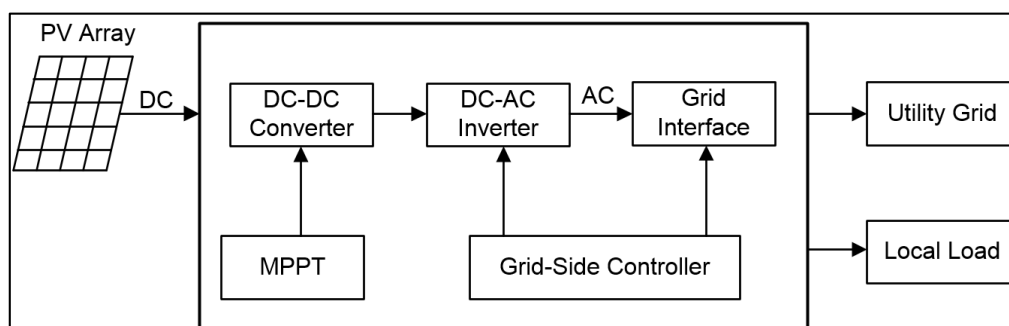
Figure 1-3 A Grid-Connected PV System

PV array is made up of a large number of PV modules. Each module consists of a group PV cells connected in series and parallel. A particular PV cell is made of semiconductor material that produces a DC voltage/current when exposed to sunlight [8].

The second part of PV system is the Maximum Power Point Tracking (MPPT) controller. At a given solar irradiance and temperature, the output power from the PV array is influenced by its output voltage. The function of the MPPT controller is to automatically find the output voltage or current at which the PV array should operate to supply the maximum power and force the PV array to work at this voltage or current [9].

The DC-DC converter converts the DC power to an appropriate voltage level required by the inverter and draws a current from the PV array suitable for maximum power [10].

The inverter is the main element in the grid-connected PV systems. The main function of the inverter is to convert the variable DC voltage output from the DC-DC converter to an AC voltage with an appropriate magnitude and frequency, and high quality (low harmonics and low Electromagnetic Interference (EMI)) that can be fed into the grid [11].

The Controller tasks in PV systems can be divided into two major parts: input-side control and grid-side control. The input-side task is to extract the maximum power from PV array, in addition to the protection of the PV array. The grid-side controller controls the inverter to regulate the DC-link voltage, in addition to controlling active and reactive power output from PV system. Besides, it is responsible for grid synchronization control and high-quality output power [12].

1.2 Research Objectives and Problem Statement

The problem to be addressed by this thesis is how to build a highly efficient model for a grid-connected PV system. Then, the developed model can be used to simulate real-life scenarios and develop advanced control and synchronization algorithms, which will yield to improved efficiency, stability, and reliability of the grid-connected PV system.

To achieve these goals, the research will be carried in the following phases:

- Conduct a literature review on the grid-connected PV system and its components,

- Modelling a PV array for grid-connected system,

- Modelling an efficient MPPT system and designing the boost converter,

- Modelling a three-phase inverter for the PV system,

- Modelling and implementing modern switching schemes to control the power electronic devices within the DC-DC converter and the inverter in a PV system,

- Implementing the synchronization process of the power electronic converter/ inverter output with a utility grid system,

- Modelling active and reactive power control algorithm,

- Testing the PV system model under various grid and weather conditions to ensure that the model is reliable, stable and controllable.

1.3 Thesis Overview

Chapter 2 covers literature review, both hardware structure for grid-connected PV system in addition to the main control and protection algorithms are discussed. In Chapter 3, modelling and simulation of PV array, boost DC-DC converter, Phase Locked Loop (PLL), MPPT controller, inverter, an inverter controller, and LCL-filter are presented. The entire model of the grid-connected PV system is presented and tested in Chapter 4. In Chapter 5, conclusions are drawn, and future work is summarized.

Chapter 2   LITERATURE REVIEW

2.1 Modelling of a Photovoltaic Cell

The Photovoltaic (PV) cell is a PN junction device made from semiconductor materials. It is commonly made of doped silicon [6]. The energy conversion in a PV cell may be described in three steps. First, the absorption of solar (photons') energy generates electron-hole pairs. Then, the electrons and holes are separated by the structure of the device. Finally, electric charges are collected at the terminal of PV cell [8]. The rate of generation of electric charge depends on the solar irradiance, the temperature of the cell and the semiconductor material type.

The output power from a single PV cell is low. A large number of PV cells are connected in series and parallel, making a PV module, to produce higher power levels. Then, several modules are connected in series and parallel to make a PV array as shown in Figure 2-1.
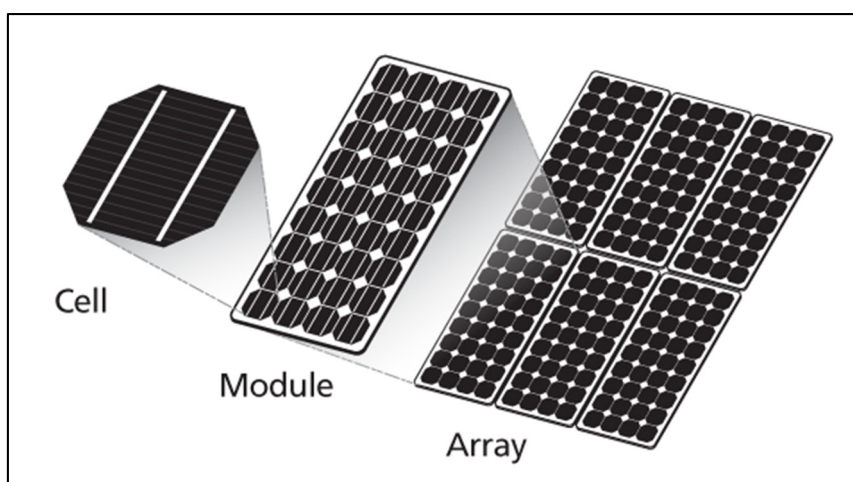
Figure 2-1 PV Cell, Module and Array [13]

2.1.1 Types of PV Cells

Different materials and technologies are used in manufacturing PV cells and modules. The PV cell technologies available in the market today can be classified into [14], [15]:

I.   Wafer-Based crystalline Silicon (c-Si) technology: either single crystalline Silicon (sc-Si) or multi-crystalline Silicon (mc-Si).The efficiency of crystalline silicon modules ranges from 19% to 24% [16].

II.   Thin-Film PV technologies. Thin-Film PV cells are made of a thin layer of semiconductor. They have lower production costs and lower cell efficiencies than wafer-based PV cells. They generally include three main families:

   a) Amorphous (a-Si) and microcrystalline Silicon (a-Si/μc-Si). Their efficiencies are up to 12% [16].

   b) Cadmium-Telluride (CdTe). Their efficiencies are up to 19% [16]

   c) Copper-Indium-Gallium-Diselenide (CIGS). The Current module efficiencies are about 18% [16].

2.1.2 PV Cell Models Overview

The basic device of a PV system is the PV cell. Therefore, in order to study and design the whole PV system, it is important to build a model for the PV cell. A reliable and accurate mathematical model of PV cell is important to design and test other parts of a PV system and to design the control algorithms of the PV system. This model is useful in studying and designing the MPPT algorithm, the inverter, the control strategy and the synchronization algorithm. Moreover, datasheets of the PV modules provide the module parameters at only Standard Test Condition (STC), so the mathematical model should use that information to predict the device's behavior at any condition accurately.

- **Ideal PV Cell Model**

Figure 2-2 shows the equivalent circuit of an ideal PV cell. The current output of a PV cell (I) is related to its voltage (V) by eq. (2-1) [17]:

$$I = I_{ph} - \underbrace{I_s \left[e^{\left(\frac{qV}{AkT} \right)} - 1 \right]}_{I_D}$$ **2-1**

where I_{ph} is the photo current (depends on the solar irradiance and cell temperature), I_D is the diode current, I_s is the diode saturation current, q is the electron charge, k is the Boltzmann constant, T is the PV cell temperature in Kelvin, and A is the diode ideality constant.

Figure 2-3 shows the I-V characteristic curves of PV cell at constant insolation and temperature.
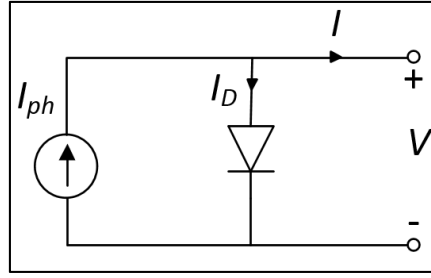
Figure 2-2 Equivalent Circuit of an Ideal PV Cell
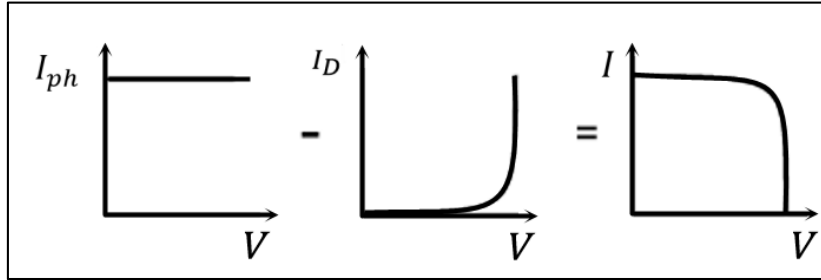
Figure 2-3 The I-V Characteristic of an Ideal PV Cell [17]

- **Practical PV Module**

A PV module is built up of several PV cells connected in series and parallel. The practical model of the PV module shown in Figure 2-4. The new parameters in the practical model are a shunt resistor (R_{sh}) to express a leakage current, and a series resistor (R_s) to represent an internal resistance of PV module and wiring [17], [18]. The current-voltage of a PV module is described by the relationship:

$$I = I_{ph} - I_s \left[e^{\left(\frac{q(V + IR_S)}{N_S AKT} \right)} - 1 \right] - \frac{V + IR_S}{R_{sh}} \qquad \textbf{2-2}$$

where N_s is the number of series connected cells, R_s is the equivalent series resistance of the module and R_{sh} is the equivalent parallel resistance. Figure 2-5 shows the I–V characteristic of the practical PV module.
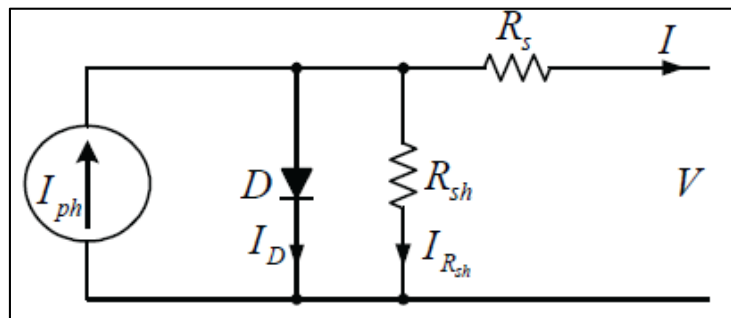
Figure 2-4 Practical PV Module [18]
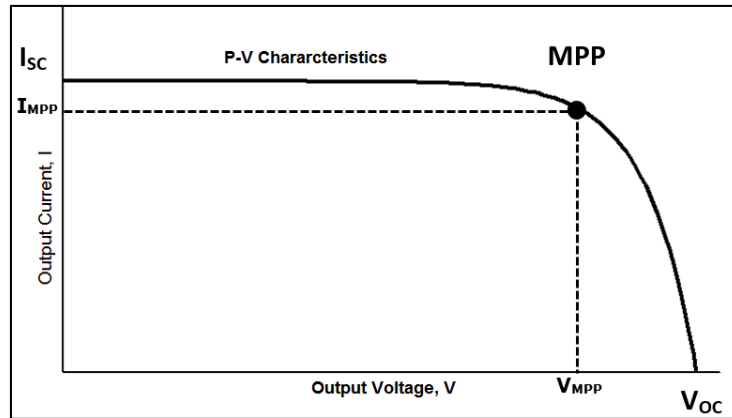
Figure 2-5 The I-V Characteristic of the Practical PV Module

2.1.3 Modelling of PV Modules

The goal of PV modelling is to find the equivalent circuit parameters (I_{ph}, I_s, R_s, R_{sh}, A) using the information given in the PV module datasheet. The parameters that are normally provided by the datasheets of the PV module are the short-circuit current (I_{sc}), the open-circuit voltage (V_{oc}), and the operating voltage and current at maximum power point (V_{mpp}, I_{mpp}). All these values are given at STC, which are a temperature of 25°C and an irradiance of 1000 Watt/m^2.

Different equivalent circuits and mathematical models have been developed for PV systems. They vary in complexity, simulation time needed and accuracy. PV models can be classified into four types:

1) The Ideal Single Diode Model (ISDM), shown in Figure 2-2. Mahmoud et al. [19] proposed ISDM, which is simple, efficient and needs less simulation time than other models.

2) The Single Diode Model (SDM), shown in Figure 2-4. Villalva et al. [17] present a SDM model, which selects an arbitrary value for the diode ideality constant (A). Then, uses the datasheet information to build four nonlinear equations, which can be solved iteratively to find the remaining equivalent circuit parameters (I_{ph}, I_0, R_s, R_{sh}).

3) Simplified Single Diode Model (SSDM). To reduce the complexity of the SDM, some studies neglect the shunt resistance (R_{sh}) of Figure 2-4 [18], [20].

4) Double Diode Models (DDMs). They include an extra diode in parallel with a diode in the circuit of Figure 2-4 to represent the effect of recombination of carriers [21]. Although this modification may improve the accuracy of the model, it is not as popular as SDM because it is more complex and needs higher computational power [22].

2.2 Control Structure for the Grid-Connected PV System

The control structure for a PV system can be divided into two main parts [12]:

1. The Input Side Controller (MPPT controller):

   The main function of this controller is to extract the maximum power from the PV array using the boost converter. This controller will be described in section 2.3 .

2. The Grid-Side Controller:

   This controller is implemented using a DC-AC inverter in addition to an LCL filter. It is responsible for:

   a. Active and Reactive powers and DC-link controller will be presented in Section 2.4 ,

   b. Synchronizing PV array with the grid will be covered in Section 2.5 ,

   c. Anti-Islanding will be discussed in Section 2.6 .

2.3 Maximum Power Point Tracking (MPPT) Controller

The second main part of PV system is MPPT controller. The MPPT controller is an essential and a very important part in any PV system. It is used to extract the maximum power from the PV array.

The output power of a PV array is influenced by solar irradiance and temperature. Figure 2-6 shows the P-V characteristics of a typical PV module at different irradiances and temperatures. Figure 2-6(a) shows the P-V characteristics at constant temperature and variable irradiances. It is obvious that the output power of PV modules increases when the irradiance increases. Figure 2-6(b) shows the P-V characteristics at constant irradiance and a variable temperature. It is clear that the output power of PV modules increases when the temperature decreases.

At constant irradiance and temperature, The PV module output power varies with the output voltage. The function of MPPT controller is to produce the control signal to the switch in the DC-DC converter, which controls the output voltage from PV module or array to ensure that the PV module or array supply its maximum power to the system at any temperature and irradiance values.
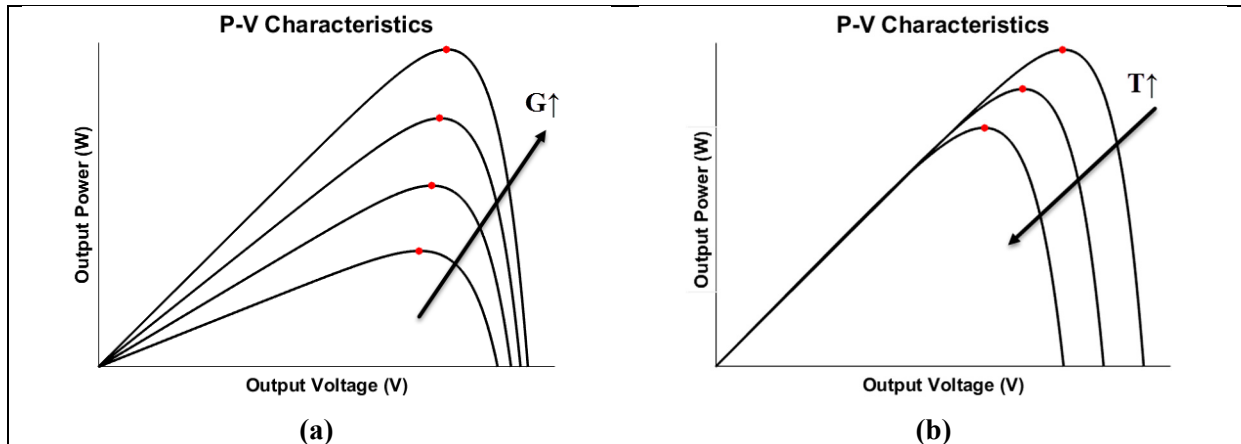
Figure 2-6 The P-V Characteristics Curve of a Typical PV Module: (a) at Constant Temperature and Variable Irradiance (b) at Constant Irradiance and Variable Temperature

2.3.1 MPPT Methods

Many MPPT methods have been reported in the literature. These methods differ from each other regarding PV array dependency, implementation complexity, accuracy, and implementation cost [23], [24].

In [23], 19 MPPT methods were reviewed, discussed and compared. The results are summarized in Table 2-1. In [24], experimental evaluation of the main MPPT techniques for PV systems was done, the results are summarized in Table 2-2. Table 2-1 and Table 2-2 can be used to select the right MPPT method for a specific PV application.

Table 2-1 Comparison between Major Characteristics of MPPT Techniques [23]

MPPT Technique	PV Array Dependent?	True MPPT?	Analog or Digital?	Periodic Tuning?	Convergence Speed	Implementation Complexity	Sensed Parameters
Hill-climbing/P&O	No	Yes	Both	No	Varies	Low	Voltage, Current
IncCond	No	Yes	Digital	No	Varies	Medium	Voltage, Current
Fractional V_{OC}	Yes	No	Both	Yes	Medium	Low	Voltage
Fractional I_{SC}	Yes	No	Both	Yes	Medium	Medium	Current
Fuzzy Logic Control	Yes	Yes	Digital	Yes	Fast	High	Varies
Neural Network	Yes	Yes	Digital	Yes	Fast	High	Varies
RCC	No	Yes	Analog	No	Fast	Low	Voltage, Current
Current Sweep	Yes	Yes	Digital	Yes	Slow	High	Voltage, Current
DC Link Capacitor Droop Control	No	No	Both	No	Medium	Low	Voltage
Load I or V Maximization	No	No	Analog	No	Fast	Low	Voltage, Current
dP/dV or dP/dI Feedback Control	No	Yes	Digital	No	Fast	Medium	Voltage, Current
Array Reconfiguration	Yes	No	Digital	Yes	Slow	High	Voltage, Current
Linear Current Control	Yes	No	Digital	Yes	Fast	Medium	Irradiance
I_{MPP} & V_{MPP} Computation	Yes	Yes	Digital	Yes	N/A	Medium	Irradiance, Temperature
State-based MPPT	Yes	Yes	Both	Yes	Fast	High	Voltage, Current
OCC MPPT	Yes	No	Both	Yes	Fast	Medium	Current
BFV	Yes	No	Both	Yes	N/A	Low	None
LRCM	Yes	No	Digital	No	N/A	High	Voltage, Current
Slide Control	No	Yes	Digital	No	Fast	Medium	Voltage, Current

Table 2-2 Evaluation Major Characteristics of MPPT Techniques [24]

Technique	Dependency of PV Array	Tracking tractor (TF)	Implementation	Accurate?	Sensors
Dcte	No	Poor	Very Simple	No	-
Vcte	Yes	Reasonable	Simple	No	V
P&O	No	Good	Simple	Yes	V, I
IC	No	Good	Medium	Yes	V, I
Modified P&O	No	Very. Good	Complex	Yes	V, I
P&O based on PI	No	Excellent	Medium	Yes	V, I
Modified IC	No	Very Good	Complex	Yes	V, I
IC based on PI	No	Excellent	Medium	Yes	V, I
Beta	Yes	Excellent	Medium	Yes	V, I
System Oscillation	Yes	Reasonable	Simple	No	V
Ripple Correlation	No	Good	Complex	Yes	V
Temperature	Yes	Very Good	Simple	Yes	V, Temperature

The most common MPPT techniques are the Incremental Conductance (IC), and Hill Climbing or Perturb and Observe (P&O) method [25], [26]. The main advantages of these methods are that they are independent of PV array, they have good performance, and they are easy to implement.

- **Hill Climbing/Perturb and Observe (P&O) Method**

The main principle of P&O method is to perturb the duty ratio of the DC-DC converter's switch and observe the output power. If the power is increasing, the perturbation should be kept in the same direction until reaching the Maximum Power Point (MPP); and if the

power is decreasing, the perturbation should be reversed to move back to the MPP [6]. Figure 2-7 visualize the P&O scheme.
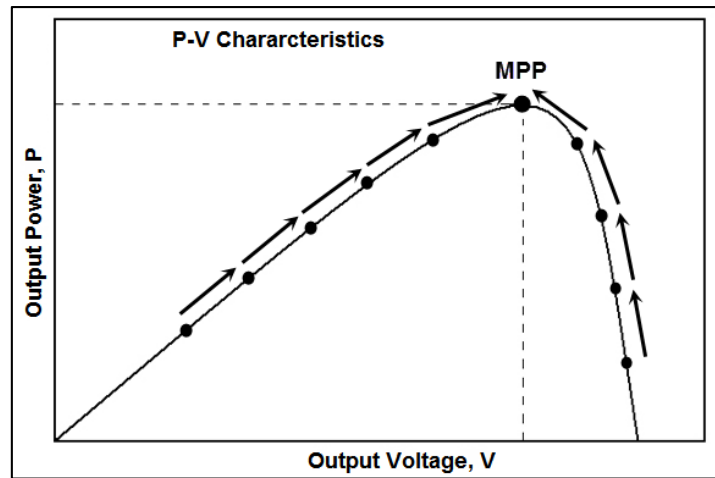
Figure 2-7 Hill Climbing/Perturb and Observe Method for MPPT

- **Incremental Conductance (IC) Method**

    The basic idea of IC method is that the slope of the power at the MPP with respect to the voltage equals zero as shown in Figure 2-8. Also, the power is increasing with the voltage to the left of the MPP, and it is decreasing to the right of the MPP. Simply, the slope of P-V characteristics curve is zero at the MPP, positive on the left of the MPP and negative on the right of the MPP [27].
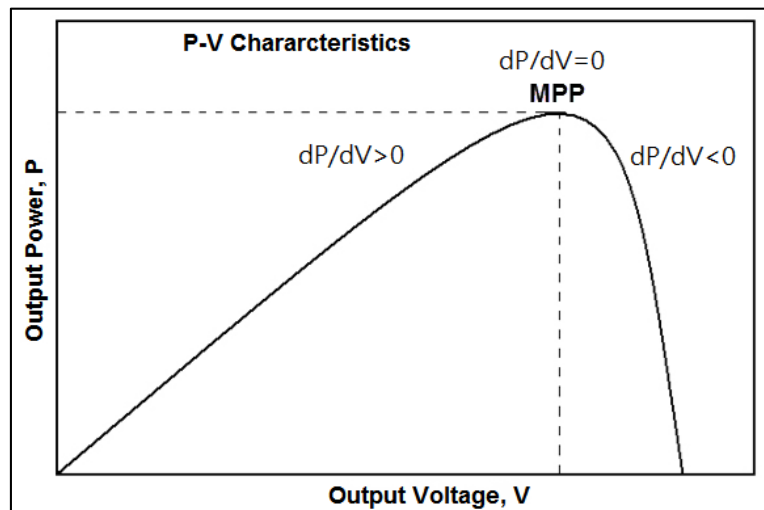
Figure 2-8 Incremental Conductance Method for MPPT

To control the output voltage of the PV array a DC-DC converter is used. Another function of the DC-DC converter is to step-up the output voltage of PV array to an appropriate voltage level required to the inverter. The most suitable DC-DC converter for PV system is the Boost (or step-up) converter [28].

2.3.2 DC-DC Boost Converter

The Boost, or step-up converter, topology used by MPPT is shown in Figure 2-9. The Boost converter is a power converter that generates output voltage greater than the input voltage. It consists of four main components: an inductor, a power electronic switch (e.g. an IGBT), a diode and a capacitor. The Boost converter is controlled using Pulse Width Modulation (PWM) control strategy. PWM controls the Boost converter by turning the switch ON or OFF at a high frequency (called the switching frequency). The description of the Boost converter and PWM is presented in detail in [29], [30]. For a continuous current conduction, the relationship between the output voltage and the input voltage is described as:

$$V_O = \frac{V_{PV}}{1-D}$$
$\qquad$ **2-3**

where V_O is the output voltage from boost, V_{PV} is the output voltage from the PV array, and D is the Duty cycle, that is equal to the fraction of time during which the switch is ON, and it has values between 0 and 1; i.e.,

$$D = \frac{T_{ON}}{T_{ON}+T_{OFF}}$$
$\qquad$ **2-4**
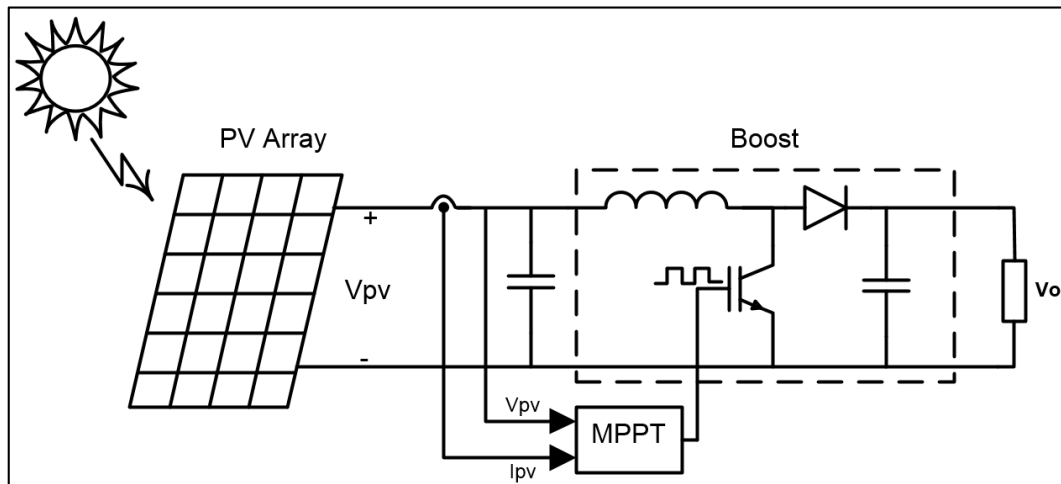
Figure 2-9 The Boost Converter Topology

2.4 Active and Reactive Powers and DC-link Controller

The controller tasks are achieved mainly by two cascaded loops [12]:

1. Fast internal current loop to control the grid current in order to get a high-quality power with low harmonics [12].

2. External voltage loop to control the DC-link voltage, which controls the power flow in the system [12].

The controller can be implemented in different reference frames:

I.   Natural Reference Frame (abc frame):

The control structure in abc frame is shown in Figure 2-10. In this controller, the DC-link voltage (U_{dc}) controller sets the active current reference (I_d*) in accordance with the required active power. In addition, the reactive current reference (I_q*) is established by the reactive power controller. The phase angle of the grid voltages (Θ) is used to create the three references for current controllers (i_a*, i_b*, i_c*) using dq to abc transformation [31]. Then, the current references are compared with the measured currents (i_a, i_b, i_c), and the error signals are fed into three current controllers. The outputs of the current controllers (U_a*, U_b*, U_c*) are used as a reference to control the three phase inverter switches [11], [12], [32].

The implementation of the current controllers can be done using Proportional Integral (PI) controller or Proportional Resonant (PR) controller. However, the nonlinear (hysteresis or dead beta) controllers are typically used due to their high dynamics [12].
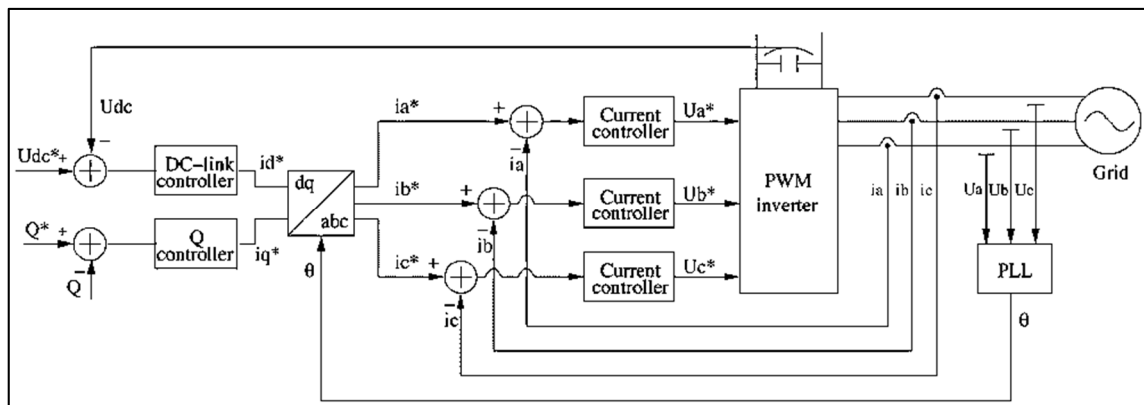
Figure 2-10 Control Structure in Natural Reference Frame [12]

II.   Synchronous Reference Frame (dq frame):

The control structure in dq frame is shown in Figure 2-11. As in natural reference frame control, the active current reference (I_d*) is generated by the dc-link voltage controller. While the reactive power controller sets the reactive current reference (I_q*). The phase angle of the grid voltages (Θ) is used to transform the grid voltages (U_a, U_b, U_c) and the grid currents (i_a, i_b, i_c) into dq frame that rotates in synchronous with the grid voltage. By mean of this, the controller variables become dc values, and this simplifies the design of controller and filter. The current controllers in the synchronous reference frame are usually implemented using a PI controller since they have a good performance when controlling DC variables [11], [12], [32].
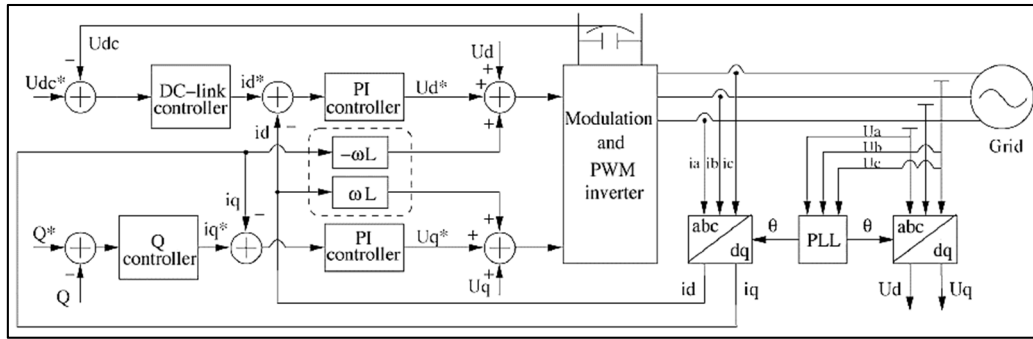
Figure 2-11 Control Structure in Synchronous Reference Frame [12]

III.   Stationary Reference Frame (αβ frame):

The control structure in a αβ frame is shown in Figure 2-12. In this structure, the grid currents (i_a, i_b, i_c) are transformed into αβ frame (i_α, i_β). Then the measured values are compared with active and reactive current references ($i_\alpha*$, $i_\beta*$) to generate the inverter control signals. The current controllers, in this case, are implemented using PR controllers [11], [12], [32].
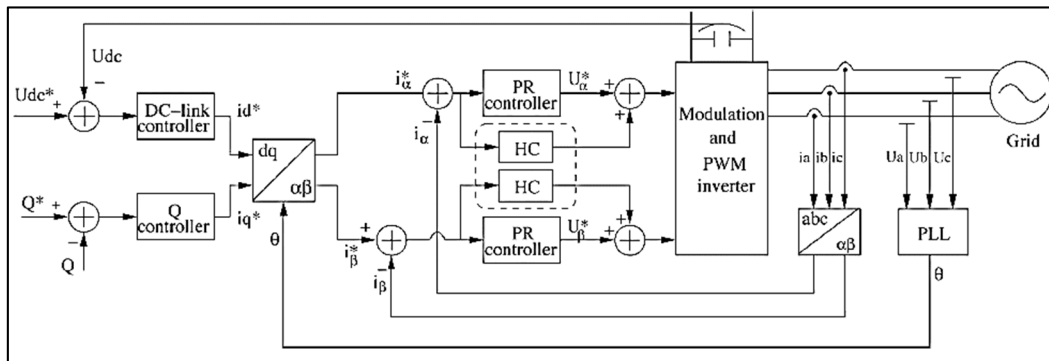
Figure 2-12 Control Structure in Stationary Reference Frame [12]

2.5 Grid Synchronization

2.5.1 Introduction

The synchronization between the PV system and the grid is one of the most important issues of the grid-connected PV systems. The main output of the synchronization algorithm is the phase angle (Θ) of the grid voltage vector. The phase angle of the grid voltage is very important for the control algorithms of grid-connected PV systems. It is used to control PV inverter switches, calculate and control of active and reactive powers, and transform the feedback variables (grid voltage and current) to a reference frame suitable for control algorithms (dq→abc or αβ→abc transformation). The synchronization algorithm for the grid-connected PV system should be able to get the phase angle even when the signal is distorted or unbalanced [12][33][34].

2.5.2 Synchronization Methods

Different synchronization methods have been developed and presented in the literature. In [11], [33], an overview of main synchronization methods is presented. In addition, a comparison of those methods is carried out. Moreover, the advantages, disadvantages, and evaluation of performance are presented. The main synchronization algorithms are Zero-Crossing Method, Filtering of Grid Voltages and Phased Locked Loop (PLL) [33], [35]. Table 2-3 shows a comparison between the synchronization algorithms.

The PLL synchronization algorithms prove to overcome the grid faults and to provide a clear synchronization signal even when the signal is distorted or unbalanced, which make them the most suitable for grid-connected applications [33], [34].

Table 2-3 Comparison between the Synchronization Algorithms [33]

Algorithm	Strong points	Weak points
$dqFilter$ (with DSC)	simplicity	on frequency shift variations
$\alpha\beta Filter$	simplicity	on unbalanced grid
$dqPLL$	works on every grid type, provides ride through capability	slow dynamics
$adaptivePLL$	estimates amplitude, frequency and phase angle	complex structure

2.5.3 The Phase Locked Loop (PLL)

The main principle of the PLL is to generate a signal to track the grid voltage signal using Voltage-Controlled Oscillator (VCO). A general structure of PLL method implemented in dq frame is shown in Figure 2-13. PLL algorithm consists of three major parts: the phase detector, the loop filter, and the VCO [11], [33], [34], [36].
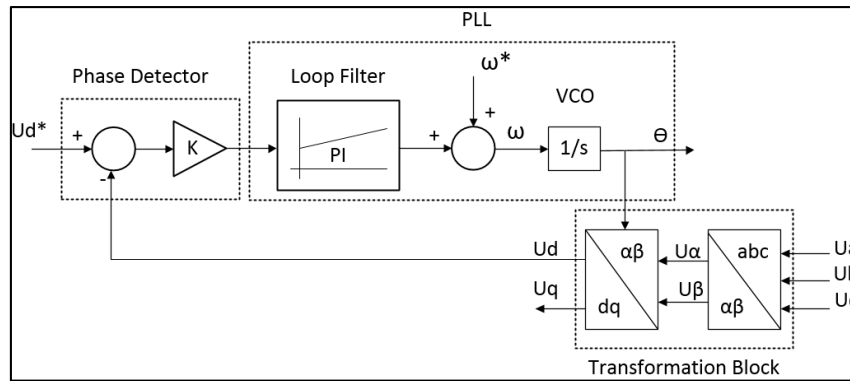
Figure 2-13 General Structure of PLL

- The Phase Detector: the phase detector outputs a signal that is proportional to the phase difference between the reference signal and the signal generated by the transformation block (abc→ dq).

- The Loop Filter: This block presents a low-pass filter, usually PI controller, to attenuate the high-frequency AC components from the phase detector output. The output of this block is the grid frequency.

- VCO: This block integrates the grid frequency to obtain the phase shift of the grid voltage (Ө).

In [37], a survey of synchronization methods for grid-connected series and shunt inverter applications was presented. Figure 2-14 summarizes those synchronization methods.
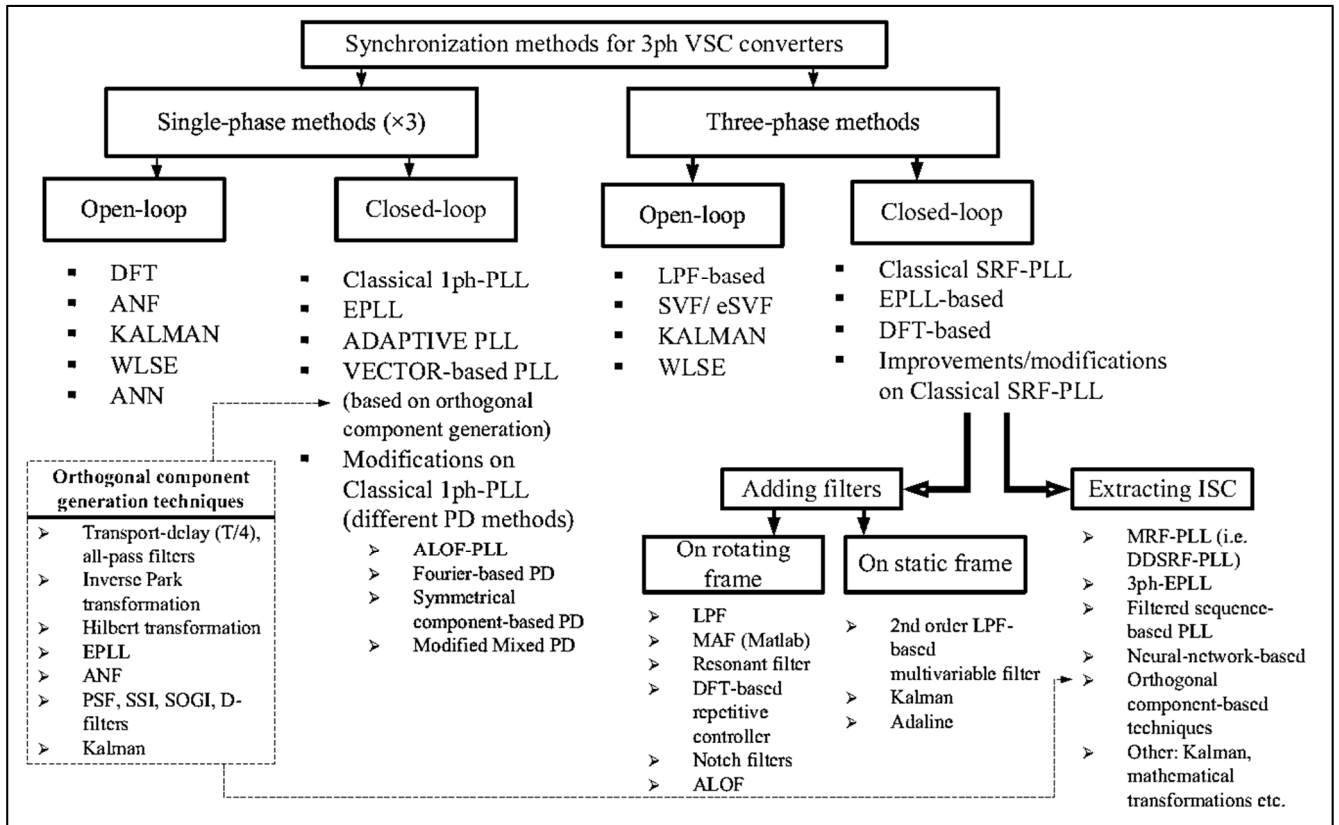
Figure 2-14 Classification of Synchronization Methods [37]

According to [37], synchronization methods can be evaluated according to dynamics/convergence time, accuracy, distortion rejection capability, noise immunity, phase and frequency adaptivity, computational burden, single or three-phase utilization, and simplicity of structure (design, tuning, and implementation).

2.6 Anti-Islanding

Anti-islanding is one of the main protection requirements for any grid-connected PV system [38]–[40]. Islanding occurs when the PV system continues to supply the local load while it is electrically isolated from the utility grid due to a grid failure or by accident. When islanding occurs, it is important to turn off the PV system to protect it along with other connected equipment. Moreover, the isolated PV system present a hazard to workers who expect the area is unpowered.

Different islanding detection techniques are presented and compared in [11], [41]–[44]. These techniques can be classified into two main groups: local or remote.

Local techniques can be divided into passive or active techniques. Passive techniques depend on the observation of system permeates at Point of Common Coupling (PCC).

These parameters could be voltage, current, frequency, harmonic distortion or power, which vary widely when the system is islanded [41], [43], [44]. Whereas, Active techniques introduce a small disturbance to some parameters and then monitor the effect in order to deduct the grid presence [42]–[44].

Remote techniques for islanding detection are based on communication system between the grid and PV system. Remote techniques are more reliable than local ones. However, they are more expensive to implement [43].

2.7 Hardware Structures for Grid-Connected PV Systems

The hardware structure of the grid-connected PV system, which used to transfer and control the generated power from the grid-connected PV system, is based mainly on power electronic devices (DC-DC converter and inverter) [45]–[49]. A classification of grid-connected PV systems is presented in Figure 2-15. In the following, a description and main characteristics of each configuration are presented:
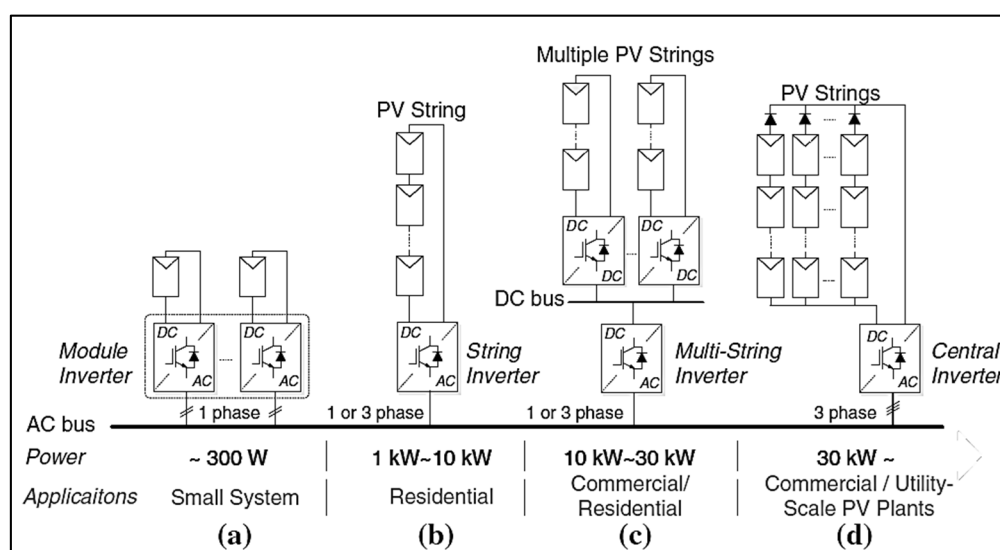
Figure 2-15 Hardware Structures for Grid-Connected PV Systems: (a) Module Inverter, (b) String Inverter, (c) Multi-String Inverter, and (d) Central Inverter [45]

- **Central Inverter Configuration (Figure 2-15(d)):**

In this configuration, a large number of PV modules are connected in series, called a PV string, which generates a high voltage that does not need amplification. Then, to produce a high power, several PV strings are connected in parallel, through a blocking diode, to form the PV array, which is attached to a three-phase central inverter [50]. The blocking diode is used to prevent power losses caused by malfunctioning or shaded strings and by a storage

system that may operate during the night [22]. The major disadvantages of this configuration are: the need for high voltage DC cables, losses in the string diodes, common MPPT, system reliability depends on one inverter, and power losses due to module mismatch [49], [50].

- **String Inverter Configuration (Figure 2-15(b)):**

In this structure, each PV string is connected to a separate single- or three-phase inverter. Then, the string inverters are paralleled and connected to the grid. If the string voltage is high enough, then there is no need for voltage boosting (more efficient). However, if the string voltage is not sufficient, then a DC-DC Boost converter, a DC-AC-DC high-frequency transformer-based converter, or a grid-side line frequency transformer is used to boost the voltage level [48], [51]. Unlike the central inverter, each string has a separate MPPT and does not need a blocking diode, which reduces the losses and improves the energy yield. Moreover, the string inverters have a lower price due to mass production. However, there are still mismatches in the PV panels connected in series [45], [49].

When galvanic isolation is not required, the transformer is usually removed to increase the efficiency of the system (1 to 2%) [11]. In this situation, "a specific design of transformerless inverters and modulation schemes are required in order to eliminate the leakage ground currents due to the parasitic capacitance between the PV panels and the ground" [51].

- **Multi-String Inverter Configuration (Figure 2-15(c)):**

This solution combines the advantages of both central inverter and string inverter; each string has a separate DC-DC converter with MPPT. Then, the DC-DC converters are connected to a common DC-AC inverter. This system is highly efficient and flexible since each string is controlled separately. In this way, PV strings having different sizes, technology, or weather conditions can be connected to a common inverter [49]. Furthermore, a possibility to extend the PV system can be easily achieved by plugging a new PV string with its DC-DC converter into the system [50].

- **Module Inverter Configuration (Figure 2-15(a)):**

It is made up of a single PV module connected to the grid through a single-phase inverter. The advantages of this inverter are that it has no mismatch losses. It also has a modular structure which simplifies the maintenance and modification of the PV system (plug and

play) [52]. However, the module inverter has a low overall efficiency caused by the high-voltage amplification. Moreover, the price per Watt is high relative to previous cases [49].

2.7.1 Grid-Connected PV System for Residential Applications

Figure 2-16 shows a typical grid-connected PV system for residential applications (several kW), it usually has three main devices: a DC-DC Boost converter, an inverter, and a filter, that is typically used at the output of the inverter to attenuate the high-frequency harmonics [51].
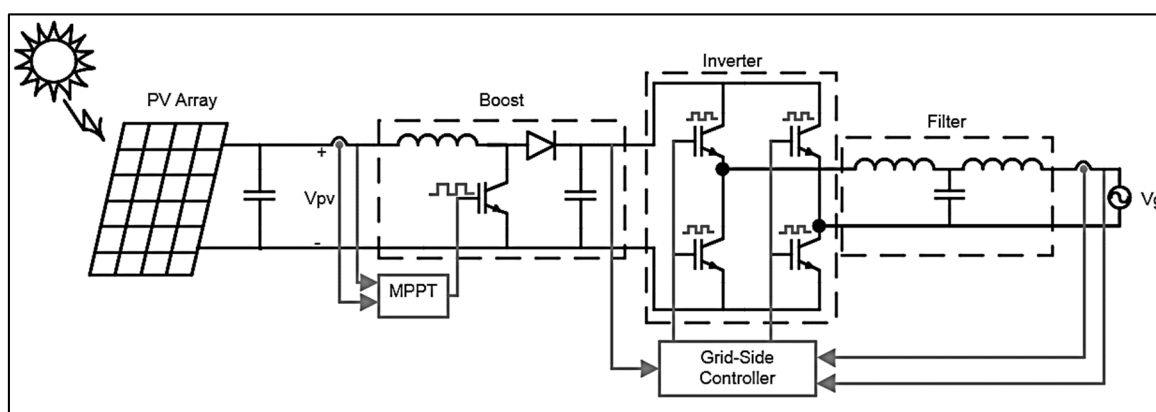
Figure 2-16 Grid-Connected PV System

2.7.2 Grid-Connected Single-Phase Inverters

The design and operation of a PV system inverter depend on the grid demand. As the demand for higher power ratings and more efficient PV system increases, new high efficient inverters are developed for PV systems, most of them are single-phase transformerless inverters. Transformerless inverters are usually based on Full-Bridge (FB) inverter, Neutral Point Clamped (NPC) inverter, or multilevel inverters [11], [50], [52]–[55]. Figure 2-17 shows two examples for single-phase transformerless inverters that are derived from FB topology. Whereas, an example for NPC transformerless inverter is shown in Figure 2-18.
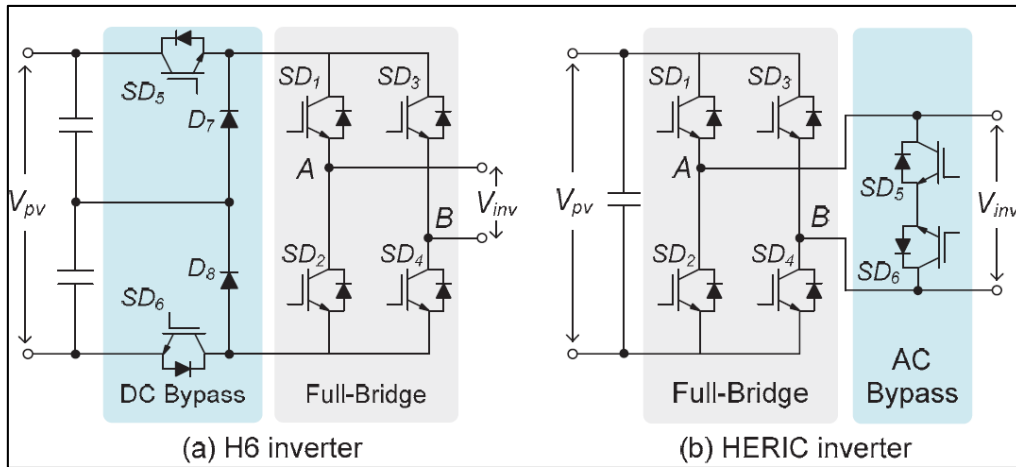
Figure 2-17 Transformerless PV Inverters Based on FB (H6 and HERIC) [45]
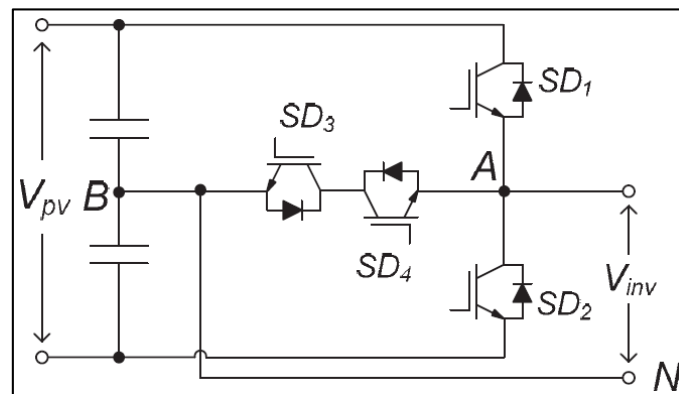
Figure 2-18 Neutral Point Clamped Transformerless Topology for PV System [45]

2.8 Grid Filter

The output voltage and current of the inverter have high Total Harmonic Distortion (THD) due to the high-frequency harmonics generated by switching frequency [30]. However, a low THD is one of the most important requirement for grid-connected systems [38]–[40]. Thus, a low-pass filter is usually used to attenuate the high-frequency harmonics. The current THD is defined as [56]:

$$THD_I = \frac{\sqrt{\sum_{n=2}^{\infty} I_n^2}}{I_1}$$

2-5

where I_1 is the rms value of the fundamental current and I_n is the rms value of the nth harmonic current.

L-filter, LC-filter or LCL-filter may be used for a grid-connected PV system. Although L-filter is simple, it requires high switching frequency to attenuate the harmonics sufficiently. However, the switching frequency is limited in high power applications. To achieve a

sufficient attenuation at a low switching frequency, a larger inductor should be used. However, this will result in poor system dynamics due to the voltage drop across the inductor [57], [58].

LC-filter is easy to design and has better attenuation factor than L-filter. However, to reduce the losses and cost the capacitance should be high, which is not recommended since it may cause an inrush current. Moreover, the resonant frequency of the LC-filter depends on the grid impedance that varies over time and therefore the LC-filter is not suitable for the grid-connected applications [57], [58].

Compared to the L-Filter and LC-Filter, the LCL-filter with the same components size can provide a lower THD and a better decoupling between the filter and the grid impedance. Therefore, the LCL-filter is the most attractive solution for grid-connected applications[57], [58]. However, LCL filter requires more complex control strategies, and various constraints have to be considered when designing the LCL-filter. These constraints include "the resonance phenomenon, the current ripple through inductors, the total impedance of the filter, the current harmonics attenuation at the switching frequency and the reactive power absorbed by capacitor" [57].

2.9 Standards

The hardware and control algorithms requirements of a grid-connected system are driven by the various standards. The standard requirements deal with issues like the response to abnormal grid conditions, power quality, grounding, and anti-islanding. In [11], [50] an overview of these standards was presented. The most important and recent standards are:

- IEEE 1547-2003 [38]: Standard for Interconnecting Distributed Resources with Electric Power Systems,

- IEC 61727 [39]: Photovoltaic (PV) Systems – Characteristics of the Utility Interface,

- VDE 0126-1-1 Safety [40]: Automatic Disconnection Device between a Generator and the Public Low-Voltage Grid.

Chapter 3 MODELLING AND SIMULATION

In Chapter 2, the literature review about the grid-connected PV system has been carried out. The main components of the grid-connected system have been presented and discussed. These components are the PV array, the DC-DC Boost converter, the MPPT controller, the VSI, the LCL filter, the PLL, and the active and reactive power controller. In this chapter, MATLAB/SIMULINK models for the system components will be developed, verified and tested.

3.1 Modelling and Simulation of a PV Module

A simple and an efficient approach proposed by [19] has been modelled using MATLAB/ SIMULINK. The proposed model is developed to estimate the equivalent circuit parameters of ISDM shown in Figure 2-2. In addition, a MATLAB/SIMULINK model for a PV module had been used in the simulation of the PV system built.

3.1.1 PV Module Modelling

The PV module equivalent circuit in Figure 2-2 can be described by [19]:

$$I = I_{ph} - \underbrace{I_s\left[e^{\left(\frac{qV}{N_S KAT}\right)} - 1\right]}_{I_D} \qquad \textbf{3-1}$$

This model has three unknowns I_{ph}, I_S and A.

I_{ph} is determined as follows [19]:

$$I_{ph} = G(I_{SC} + \alpha\Delta T) \qquad \textbf{3-2}$$

Where G the solar irradiance (kW/m^2), I_{SC} is the short circuit current at STC, which is given in the datasheet, ΔT is the difference between the module temperature and the STC temperature (25^oC), and α is the current temperature coefficient provided in the product datasheet. Evaluating eq. (3-1) at STC (G=1 and T=25^oC) and V=V_{oc} yields:

$$I_{rs} = \frac{I_{sc}}{\left[e^{\left(\frac{qV_{oc}}{N_S KAT_o}\right)} - 1\right]} \qquad \textbf{3-3}$$

where I_{rs} is the is the saturation current at STC.

By evaluating eq. (3-1) at STC and Maximum Power Point (MPP) yields [19]:

$$I_{rs} = \frac{I_{sc} - I_m}{\left[e^{\left(\frac{qV_m}{N_s KAT_o}\right)} - 1 \right]}$$

3-4

- Equations (3-3) and (3-4) can be solved to get the diode ideality factor "A" [19].

- To Find the Is:

$$V_{OC}(G,T) - V_{OC}(G,T_o) = -|\beta|\Delta T$$

3-5

where $V_{OC}(G,T)$ is the open circuit voltage at current temperature and irradiance, $V_{OC}(G,T_o)$ is the open circuit voltage at STC temperature (25°C) and current irradiance, β is the temperature coefficient of V_{OC} (given by datasheet) [19].

By substituting I=0 in eq. (3-1), the open circuit voltage formula is determined as [19]:

$$V_{OC}(G,T) = \frac{N_s KTA}{q} ln(\frac{I_{ph}}{I_s} + 1)$$

3-6

Substituting eq. (3-2) in eq. (3-6) yields:

$$V_{OC}(G,T) = \frac{N_s KTA}{q} ln(\frac{G(I_{SC} + \alpha \Delta T)}{I_s} + 1)$$

3-7

By evaluating eq. (3-7) at T and T_o and substituting in eq. (3-5) yields:

$$\frac{N_s KA}{q} \left[T ln \left(\frac{G(I_{SC} + \alpha \Delta T)}{I_s} \right) + 1 - T_o ln \left(\frac{GI_{SC}}{I_{rs}} + 1 \right) \right] = -|\beta|\Delta T$$

3-8

By rearranging eq. (3-8), I_S can be expressed as:

$$I_S = \frac{I_{ph} e^{\left(\frac{|\beta|\Delta T q}{N_s KAT}\right)}}{\left(\frac{GI_{SC}}{I_{rs}} + 1\right)^{\frac{T_o}{T}} - e^{\left(\frac{|\beta|\Delta T q}{N_s KAT}\right)}}$$

3-9

The modelling of the PV module using SIMULINK is described in the following steps:

1. The temperature and irradiance level are the two inputs of the PV module. As shown in Figure 3-1, the module temperature is converted from Celsius (°C) to Kelvin, and the Irradiance level is converted from W/m² to kW/m².
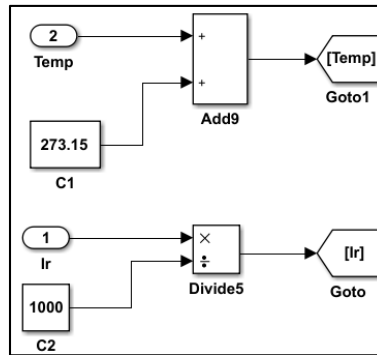
Figure 3-1 Current and Temperature Conversion SIMULINK Block Diagram

2. Figure 3-2 shows the SIMULINK block diagram used to find the photo current (I_{ph}). The converted values of temperature and irradiance level together with the value of current temperature coefficient (from PV module datasheet) are used to calculate the photo current (I_{ph}) using eq. (3-2).
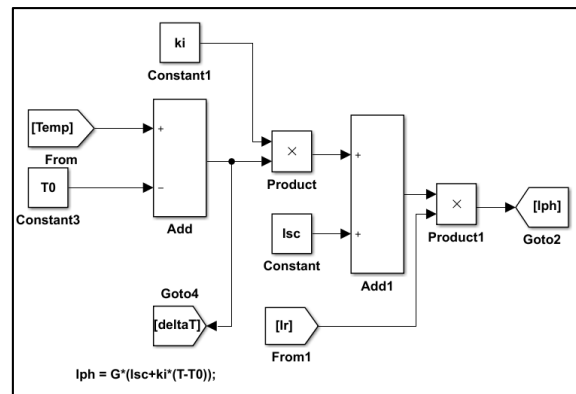
**Figure 3-2 Block Diagram to Find the Photo Current (I_{ph})**

3. The block diagram used to determine the saturation current at STC (using eq. (3-4)) is shown in Figure 3-3.
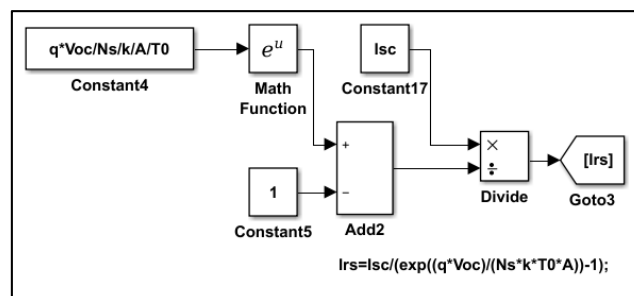

Figure 3-3 Block Diagram to Calculate the Saturation Current at STC (I_{rs})

4. The diode saturation current (I_S) which is calculated using the eq. (3-9) is presented by the SIMULINK block diagram shown in Figure 3-4
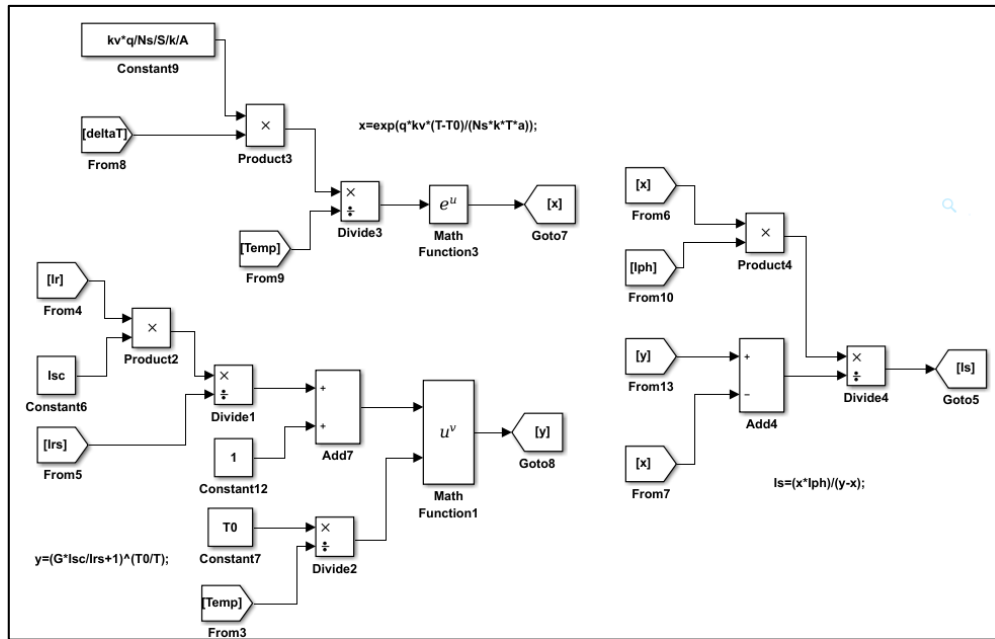
Figure 3-4 Block Diagram to Calculate the Saturation Current (I_s)

5. Figure 3-5 shows the MATLAB code used to solve eq. (3-3) and eq. (3-4) to get the diode ideality factor "A".

```
>> Vmpp = 26.3;        %voltage at Maximum Power Point
Impp = 7.61  ;       %current at Maximum power point
Voc = 32.9 ;         % Open circuit voltage
Isc  = 8.21 ;        % Short circuit current
T0=25+273.15 ;        % Temperature in Kelvin
q=1.60217646e-19;    %electron charge,
K=1.3806503e-23 ;    %Boltzmann constant
Ns=54;
syms A;
x=(q*Voc)/(Ns*K*A*T0);
y=(q*Vmpp)/(Ns*K*A*T0);
eq1=Isc/(exp(x)-1);
eq2=(Isc-Impp)/(exp(y)-1);
eq=eq1-eq2==0;
A=vpasolve(eq,A)
 A =
 1.8183572154381892946225061408685
```

Figure 3-5 MATLAB Code Used to Find the Diode Ideality Factor "A"

6. From the previous steps, the values of the photo current (I_{ph}), the diode saturation current (I_S), and the ideality factor "A" were calculated. All these values are substituted in Eq. (3-1) to calculate the output current. The SIMULINK block diagram shown in Figure 3-6 represents Eq. (3-1).
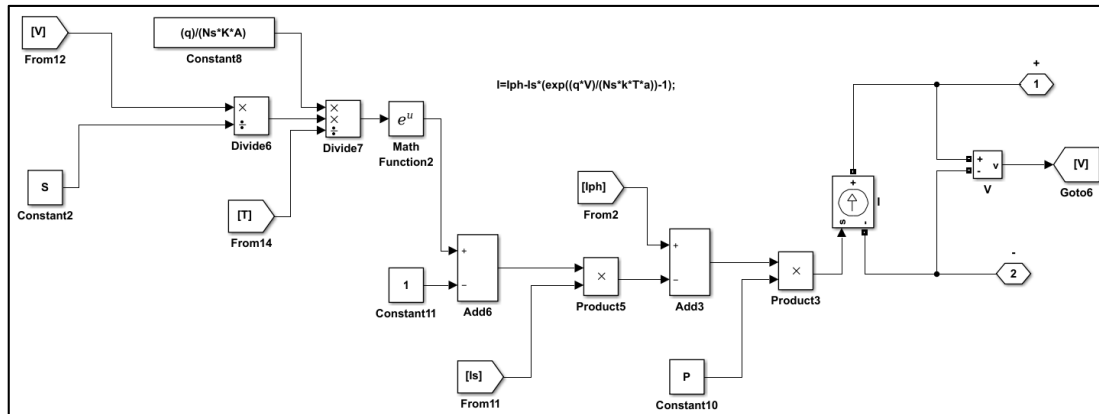
Figure 3-6 Block Diagram to Calculate the Output Current

The above model is used to obtain the equivalent circuit parameters of KC200GT PV module [59]. The values of unknowns at STC are:

$$I_{ph} = 8.21 \text{ A}$$

$$I_S = 1.78 \times 10^{-5} \text{A}$$

$$A = 1.82$$

3.1.2 Simulation

Figure 3-7 shows the SIMULINK circuit used to find the characteristics curves of the PV modules. The MATLAB code which was used to obtain the characteristics curves can be found in Appendix A.1
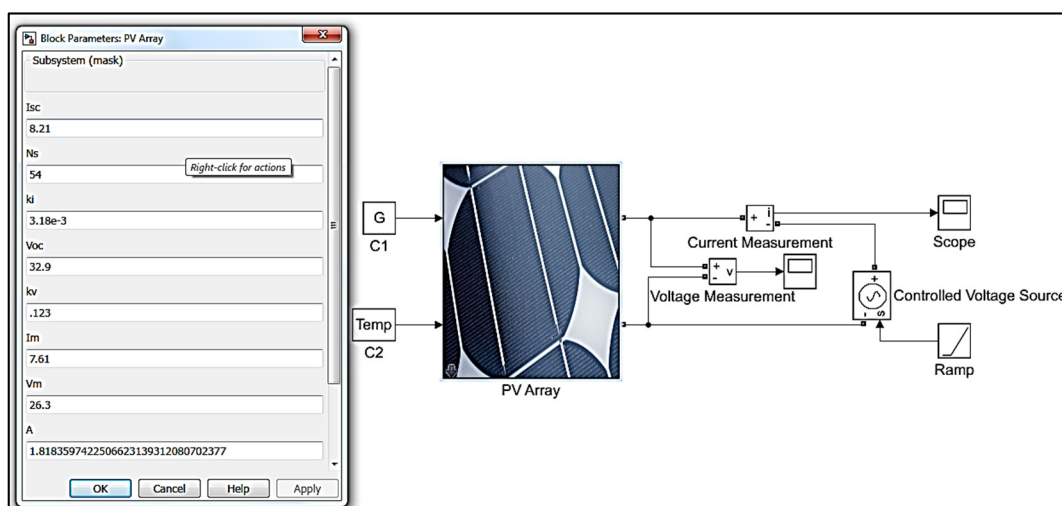
Figure 3-7 PV Module Test Circuit

The simulation results of the PV module in MATLAB/SIMULINK are shown in Figure 3-8 to Figure 3-11. In Figure 3-8, plots of I-V characteristics of the PV module are obtained, which are very similar to the actual behavior of a real PV module under the effect of various levels of irradiance. While, Figure 3-9 shows the I-V characteristics of the PV module for different temperatures, which are very close to the actual behavior of a real PV module under same conditions. Figure 3-10 shows the P-V characteristics of the PV at constant temperature and various levels of irradiance. It is obvious from the figure that the output power of PV modules increases when the irradiance increases. Figure 3-11 shows the P-V characteristics of the PV at constant irradiance and different temperatures. It is clear from the figure that the output power of PV modules increases when the temperature decreases.
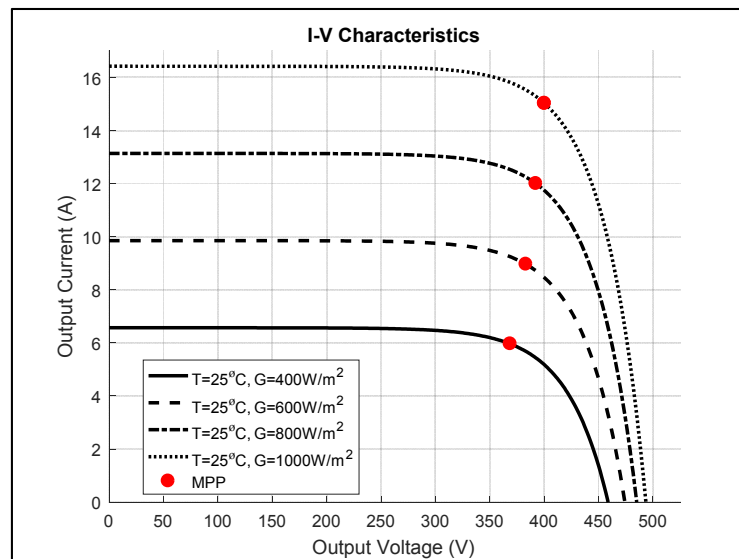
Figure 3-8 I–V Characteristic at Different Irradiances (G) and Constant Temperature (T)
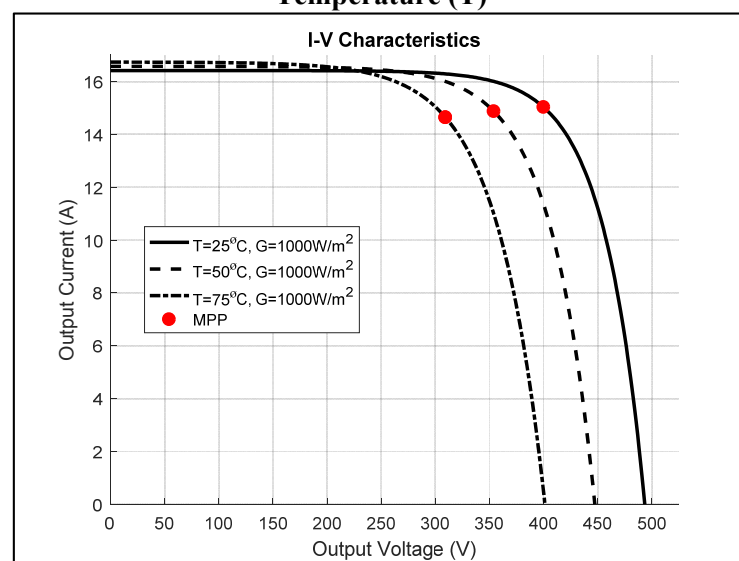
Figure 3-9 I–V Characteristic at Different Temperatures (T) and Constant Irradiances (G)
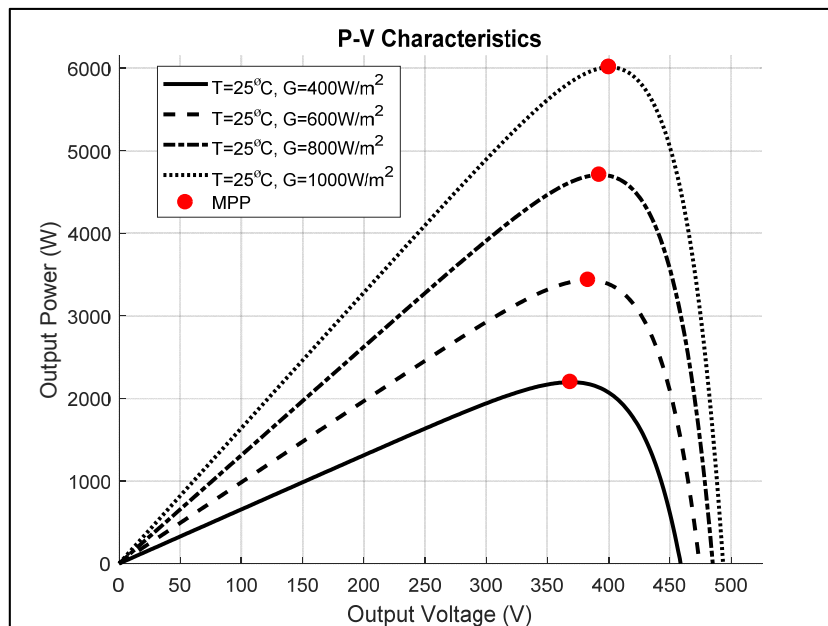
Figure 3-10 P–V Characteristic at Different Irradiances (G) and Constant Temperature (T)
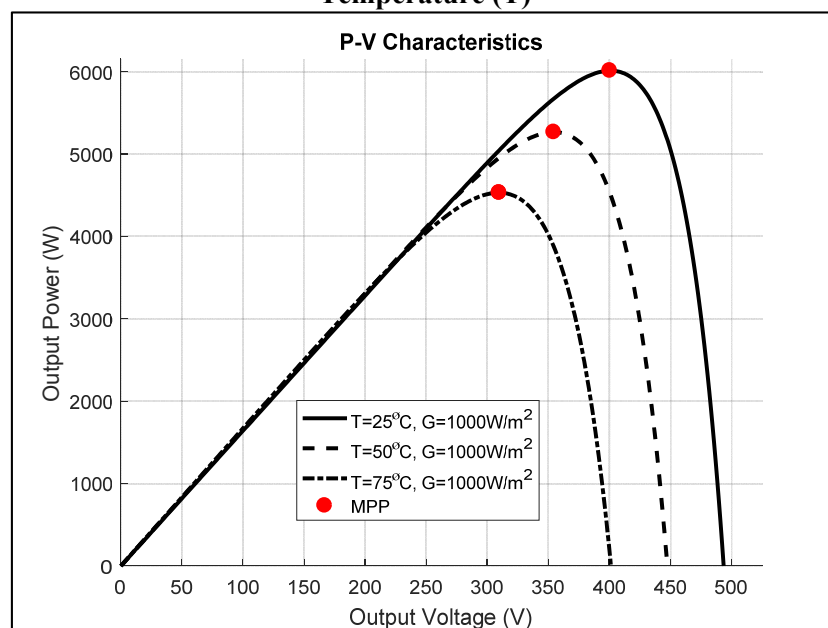
Figure 3-11 P–V Characteristic at Different Temperatures (T) and Constant Irradiance (G)

3.1.3 Validation

Figure 3-12 and Figure 3-13 shows the datasheet I-V characteristics of PV module [59]. By comparing the datasheet results with the created PV module results (Figure 3-8 and Figure 3-9), it is obvious that the simulation results match well the characteristics of the PV module in the datasheet.
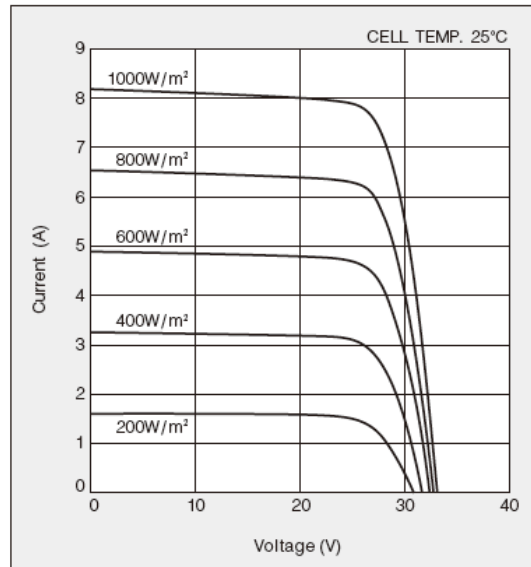
Figure 3-12 I–V PV Datasheet Characteristic at Different Irradiances, T=25ºC
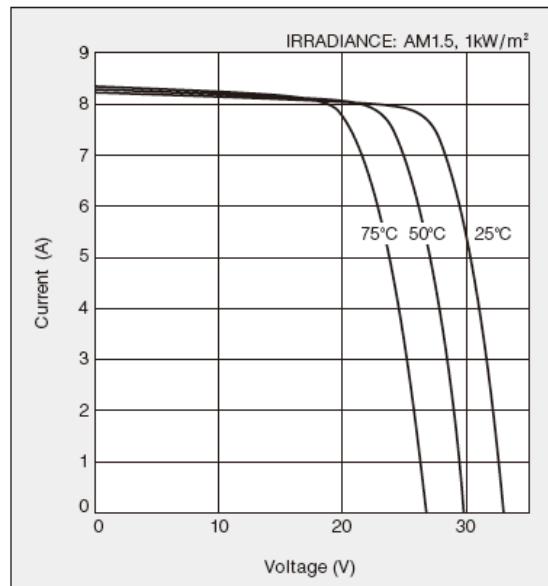
Figure 3-13 I–V PV Datasheet Characteristic at Different Temperatures, G=1000W/m²

3.1.4 PV Array Modelling

The model of the PV module can be expanded to model the PV array by setting the value of I_{ph}, I_S and V in eq. (3-1) as follows [60]:

$$I'_s = p.I_s \qquad\qquad \textbf{3-10}$$

$$V' = V\ /\ S \qquad\qquad \textbf{3-11}$$

where the S is the number of series modules, and p is the number of parallel modules.

The KC200GT module has a maximum power of 200Wp at STC as shown in Figure 3-13. To get 6kW, a PV array was constructed using 2 PV strings each of them consists of 10 modules connected in series. The I-V and P-V characteristics curves at STC are shown in Figure 3-14

(a)   **(b)**
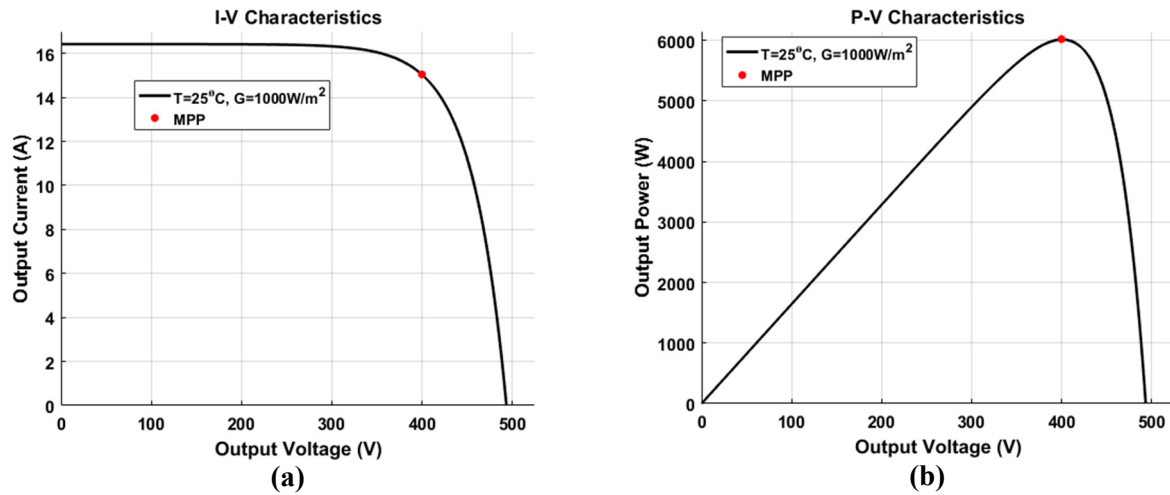
Figure 3-14 PV Array Characteristic Curves at STC: (a) I-V Characteristic Curve (b) P-V Characteristic Curve

3.2 Boost Converter

The boost converter SIMULINK model is shown in Figure 3-15. It was designed to operate in Continuous Conduction Mode (CCM) using the following equations [61];

$$L > \frac{D(1-D)^2 T_S V_o}{2 I_o}$$ **3-12**

$$C = \frac{D T_S}{R \frac{\Delta V_o}{V_o}}$$ **3-13**
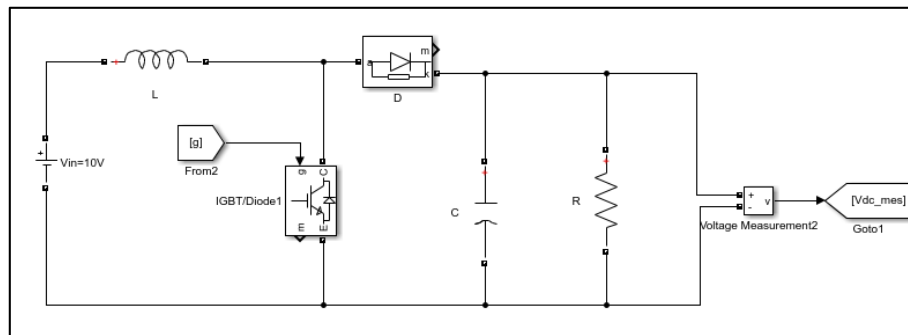
Figure 3-15 The SIMULINK Model of the Boost Converter

The closed loop control system of the Boost converter is shown in Figure 3-16. The Boost converter's output is controlled by a PI controller. The PI controller is designed using MATLAB PID tuner as shown in Figure 3-17. The MATLAB code for Boost transfer

function is shown in Figure 3-18.The derivation of the transfer function can be found in [62].
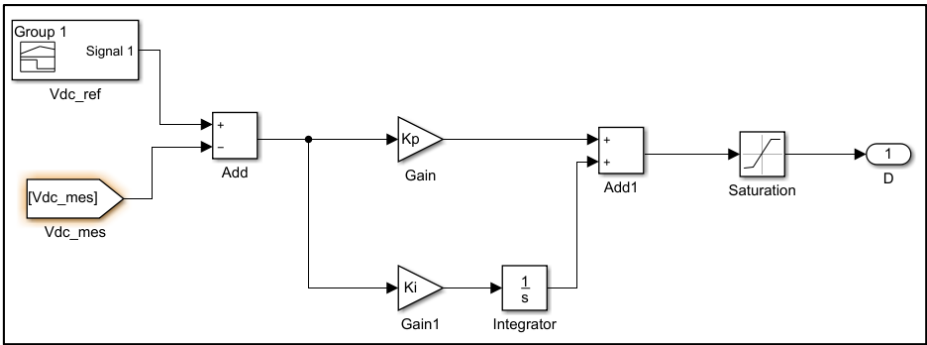
Figure 3-16 The Boost Control Circuit
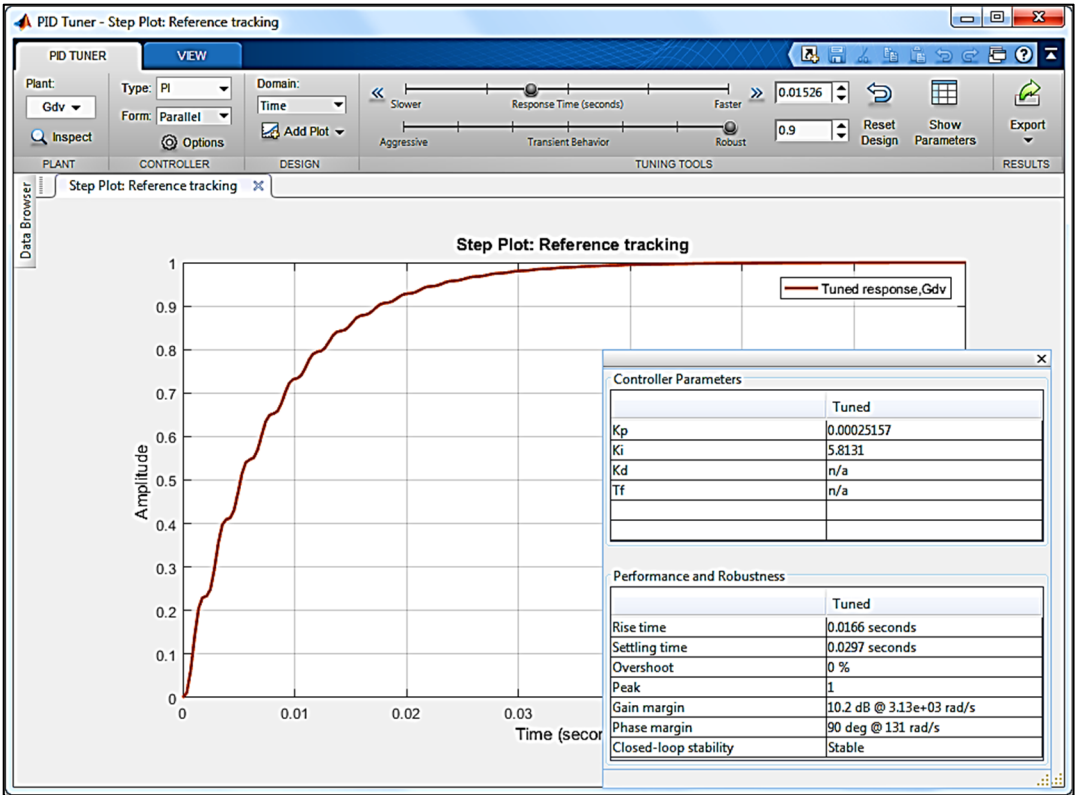
Figure 3-17 The Design of the PI Controller Using MATLAB PID Tuner

Figure 3-18 The Transfer Function of the Boost Converter

To test the Boost converter, a variable magnitude reference voltage is applied to the controller, and the output is observed. The test result is shown in Figure 3-19; the result shows that the system is stable and has a zero-steady state error. However, during transitions, there is a delay in the response.
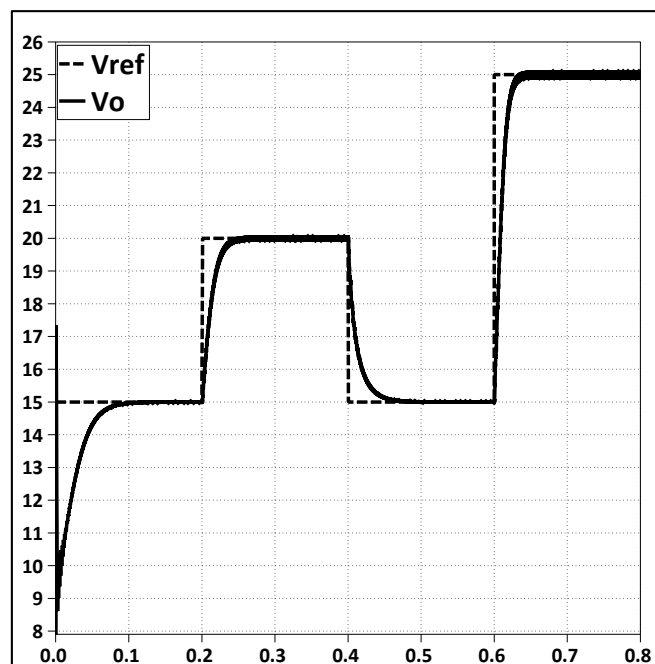
Figure 3-19 The Reference Voltage and the Output Voltage of the Boost

Another test was done by applying a variable input to the Boost and observing the output voltage while keeping the reference voltage constant. The test result is shown in Figure 3-20. The result shows that the system is stable; its output voltage has a small steady state error for a ramp input, a fast response, and an overshoot for the step change in the input voltage.
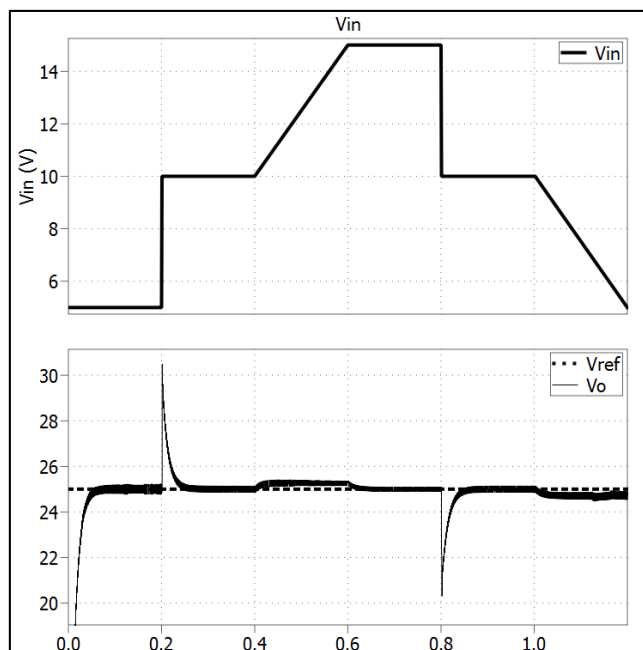
Figure 3-20 The Input, Output and the Reference Voltage of The Boost

3.3 MPPT Implementation

The flowchart of the P&O MPPT control method is shown in Figure 3-21. The MATLAB code to implement this method can be found in Appendix A.2.
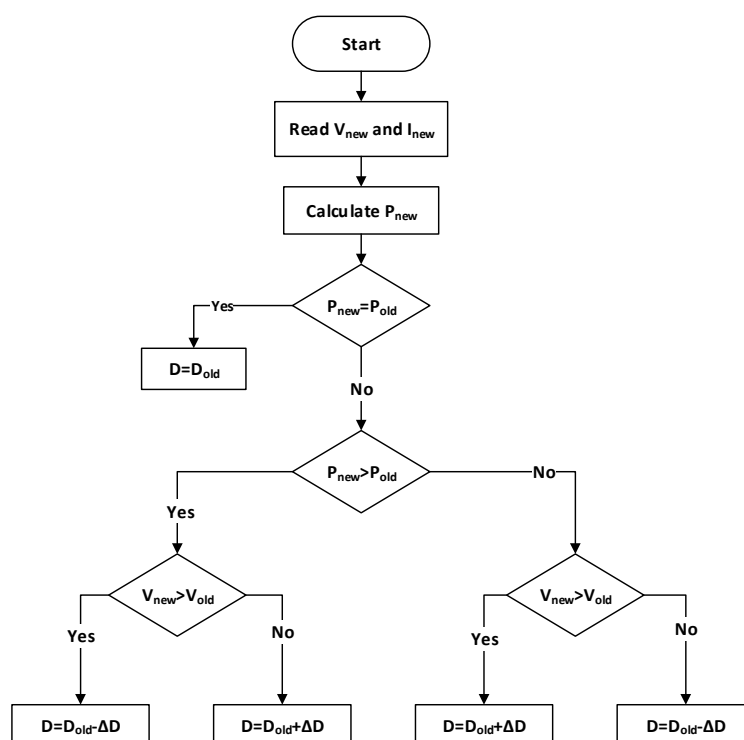
Figure 3-21 Flow Chart of P&O MPPT Algorithm

The MPPT controller used to control the duty cycle of the Boost converter switch to extract the maximum power from the PV array. Figure 3-22 shows the SIMULINK circuit used to test the MPPT algorithm.
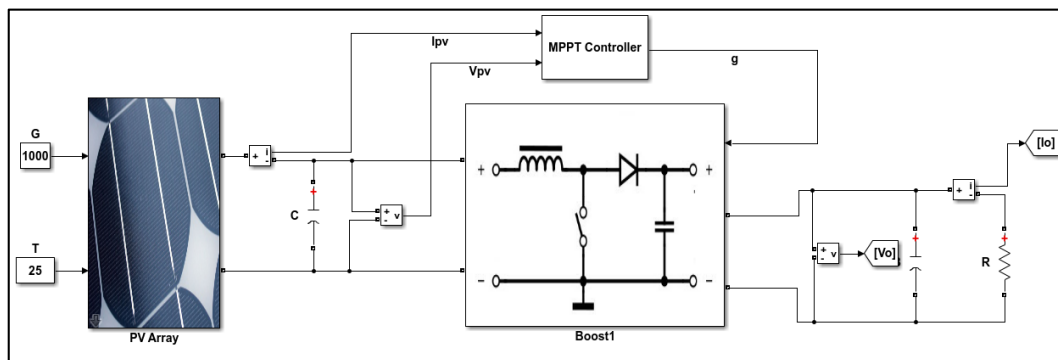
Figure 3-22 SIMULINK Circuit to Test MPPT Algorithm

Figure 3-23 illustrates the operation of the MPPT controller and Boost converter. It is obvious from the figure that when the MPPT controller is enabled at t=0.4s, it controls the duty cycle of the Boost converter to operate the PV array at the maximum power point. In addition, by comparing the input voltage (V_{PV}) with the output voltage (V_o) in Figure 3-23, the boosting action of the converter is obvious.
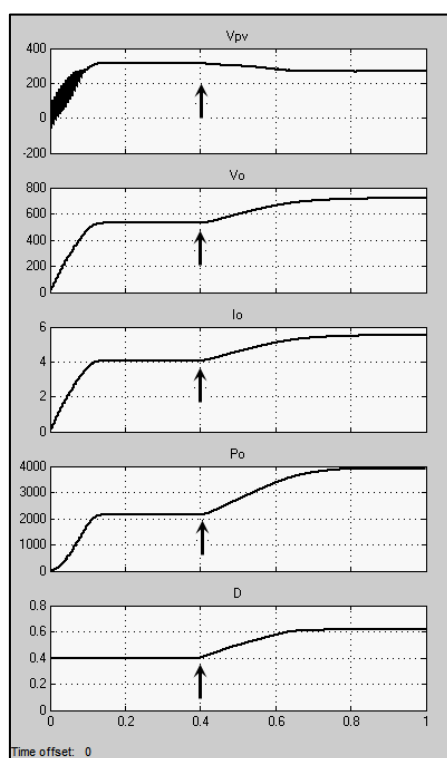
Figure 3-23 Boosting and MPPT Test

Another test was done by applying variable temperature and irradiance to the PV array and then observing the output power from the PV array. Figure 3-24 shows the test results. To verify the MPPT algorithm, the test results were compared with the data from the P-V Characteristic of the PV module (Figure 3-10 and Figure 3-11). Table 3-1 summarizes the results and shows that the MPPT algorithm success in tracking the PV module maximum power. Clearly, the MPPT forces the system to operate at the maximum power point.
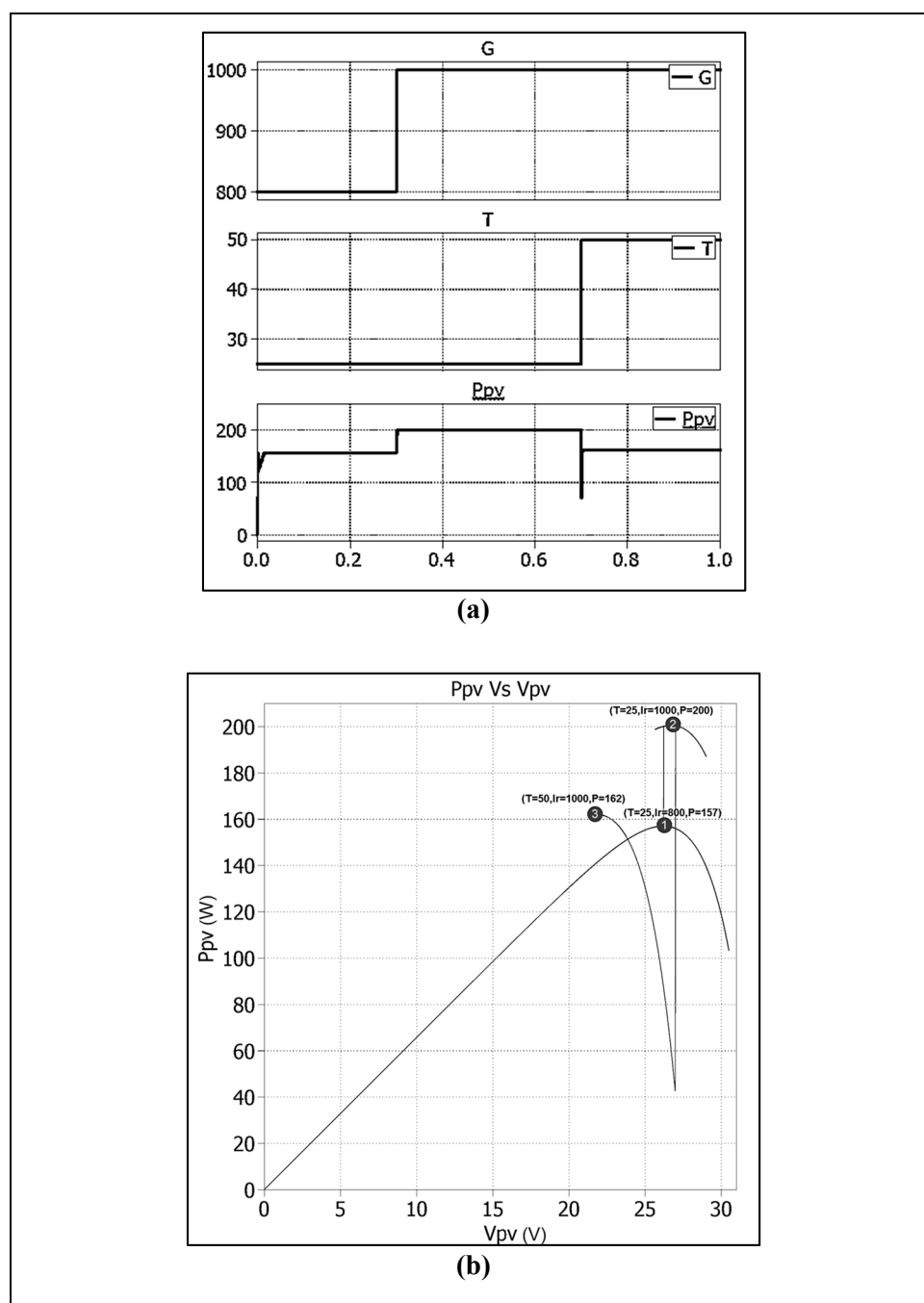
Figure 3-24 MPPT Test Results (a) PV Power for Variable T and G (b) PV Power vs. V$_{pv}$ Power for Variable T and G

Table 3-1 Results of MPPT Algorithm Test

Temperature (°C)	Irradiance (W/m^2)	Power from MPPT test (W)	Power from P-V characteristic curves (W)
25	800	157	157
25	1000	200	200
50	1000	162	162

3.4 Three-Phase Inverter

The PV array outputs DC energy, but the grid energy is AC. To transfer the generated energy to the grid, it should be converted into AC energy with controllable magnitude, phase, and frequency. To achieve this, a three-phase Voltage Source Inverter (VSI) was used. The SIMULINK circuit used to test the VSI is shown in Figure 3-25. The VSI switches are controlled using Space Vector Pulse Width Modulation (SVPWM) [63]. The SVPWM technique is widely used to control the VSI. Compared to the sinusoidal pulse width modulation (SPWM), SVPWM is more suitable for digital implementation and it has better dc-link voltage utilization. Moreover, it has lower total harmonic distortion [64].

The output waveforms of voltages and currents are shown in Figure 3-26. The relationship between the DC input and the AC output line-to-line voltage is given by:

$$V_{LLrms} = 1.15 \times \frac{M\,V_{DC}}{2} \times \frac{\sqrt{3}}{\sqrt{2}} \qquad \qquad \textbf{3-14}$$
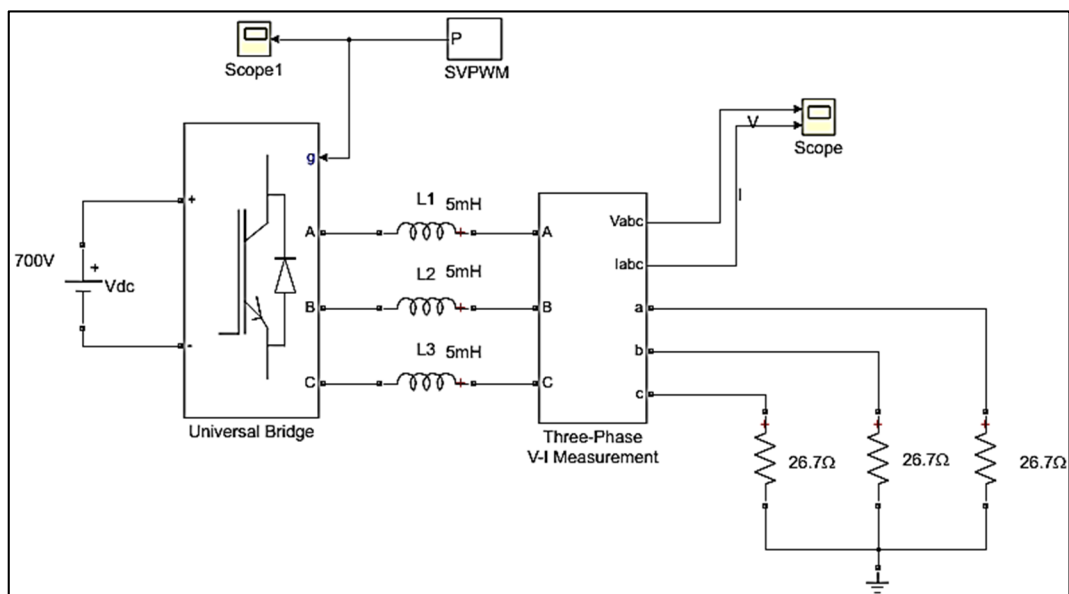
Figure 3-25 SIMULINK Circuit for the VSI
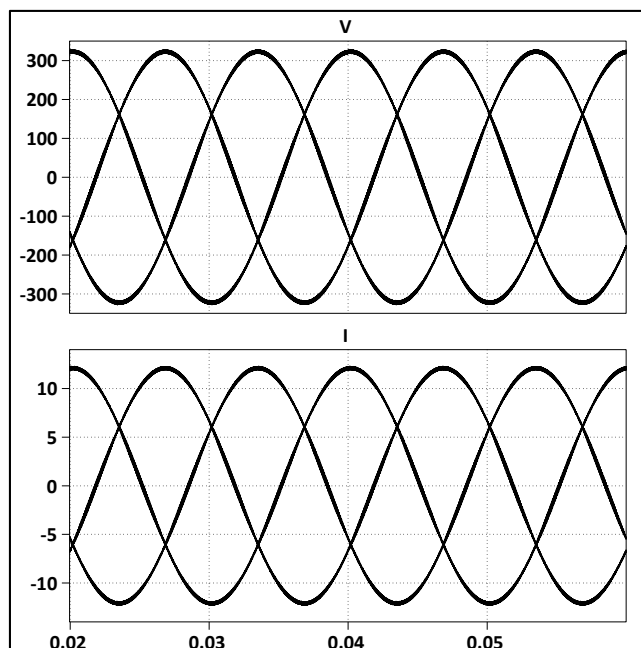
Figure 3-26 DC-AC Conversion

3.5 LCL Filter Design

The LCL-filter is used to attenuate the high-frequency harmonics of the output current. The circuit diagram of the LCL-filter is shown in Figure 3-27.
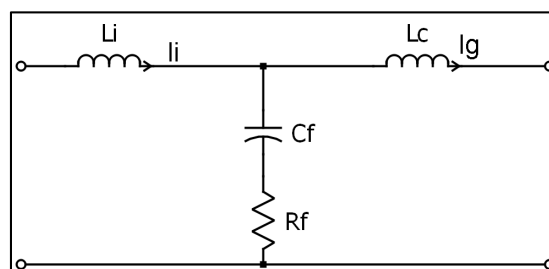
Figure 3-27 Circuit Diagram of the LCL-filter

The design procedure of the LCL-filter can be described by the following steps [56], [65]–[67]:

1. The filter capacitance is selected based on the limit of the reactive power absorbed by the capacitor. Generally, it should be less than 5% of the rated power. The value of capacitance is given by [65]:

$$C_f = xC_b \hspace{3cm} \textbf{3-15}$$

where C_b is the base capacitance, and x is the percentage of the reactive power absorbed at rated condition. The base capacitance of the system can be calculated by:

$$Z_b = \frac{V_{LLrms}{}^2}{P_{rated}} \tag{3-16}$$

$$C_b = \frac{1}{2\pi f_g Z_b} \tag{3-17}$$

where V_{LLrms} the rms value of line to line voltage, P_{rated} is the rated power of the system, Z_b is the base impedance and f_g is the grid frequency.

2. The inverter side inductor (L_i) used to reduce the ripple of the inverter current and it is calculated using the relationship between the ripple current and the inverter inductor [65]:

$$\Delta_i = \frac{V_{DC}}{8 L_i f_{sw}} \tag{3-18}$$

where Δi is ripple current, usually limited to 10%-25% of rated current [65], f$_{sw}$ is the switching frequency. For Δi equal 20% of rated current, the value of grid inductor is given by:

$$L_i = \frac{V_{DC}}{8 f_{sw}(20\% I_b)} \tag{3-19}$$

where I$_b$ is the base current and given by:

$$I_b = \frac{P_{rated}}{\sqrt{3} V_{LLrms}} \tag{3-20}$$

3. The grid side inductance (L$_g$) can be found based on the required Ripple Attenuation Factor (RAF) at switching frequency. RAF is the ratio of grid current to the inverter output current, and it is given by eq. (3-21). RAF at switching frequency is given by eq. (3-22), which can be rewritten as eq. (3-23) to calculate L$_g$ [56].

$$RAF = \left|\frac{I_g(s)}{I_i(s)}\right| = \frac{1/(L_g C_f)}{s^2 + 1/(L_g C_f)} \tag{3-21}$$

$$RAF_{sw} = \left|\frac{I_g(s)}{I_i(s)}\right| = \frac{1}{1 - \omega^2{}_{sw} L_g C_f} \tag{3-22}$$

$$L_g = \left|\frac{I_g(s)}{I_i(s)}\right| = \frac{RAF_{sw} + 1}{RAF_{sw} \omega^2{}_{sw} C_f} \tag{3-23}$$

4. To reduce the ac voltage drop, the value of filter inductance (L_g+L_i) should be less than 0.1pu [56].

$$L_g + L_i < 0.1L_b \qquad\qquad \textbf{3-24}$$

$$L_b = \frac{Z_b}{2\pi f_g} \qquad\qquad \textbf{3-25}$$

5. The resonance frequency, which is given by eq. (3-26), should be far away from the grid frequency and switching frequency. A suitable range of f_{res} is given by eq. (3-27) [68]

$$f_{res} = \frac{1}{2\pi}\sqrt{\frac{L_i+L_g}{L_iL_gC_f}} \qquad\qquad \textbf{3-26}$$

$$10f_g < f_{res} < \frac{f_{sw}}{2} \qquad\qquad \textbf{3-27}$$

6. To avoid resonance phenomenon, a damping resistor (R_f) is usually connected in series with filter capacitor. The value of the damping resistor should be [57]:

$$R_f = \frac{1}{3(2\pi f_{res})C_f} \qquad\qquad \textbf{3-28}$$

where f_{res} is the resonant frequency.

The effect of the damping resistor on the transfer function of the LCL filter is illustrated in Figure 3-28. Figure 3-28 (a) shows the Bode plot of the filter transfer function without a damping resistor. Figure 3-28 (b) shows how the damping resistor prevents resonance in the filter.
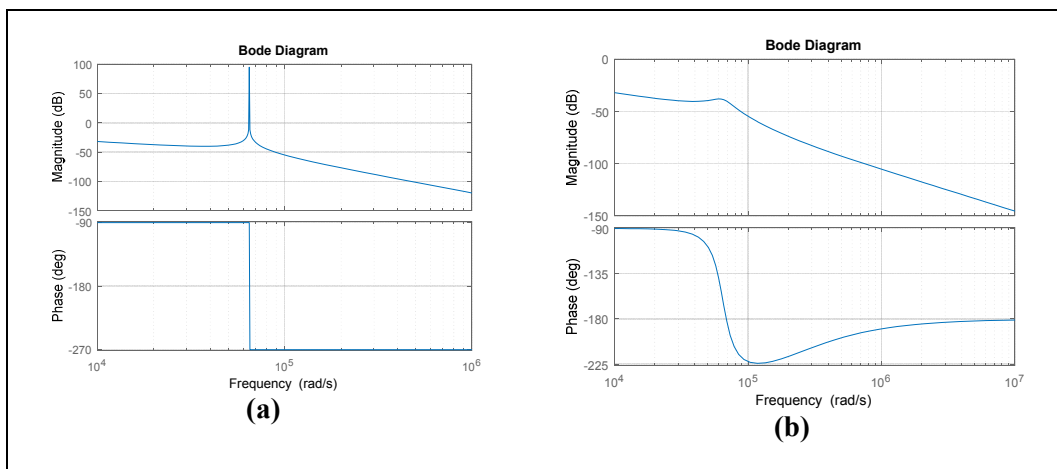
Figure 3-28 Bode Plots of the LCL filter (a) without the Damping Resistor (b) with the Damping Resistor

The flowchart in Figure 3-29 illustrates the procedure for an LCL-filter design. The MATLAB code used to design the filter can be found in Appendix A.4.
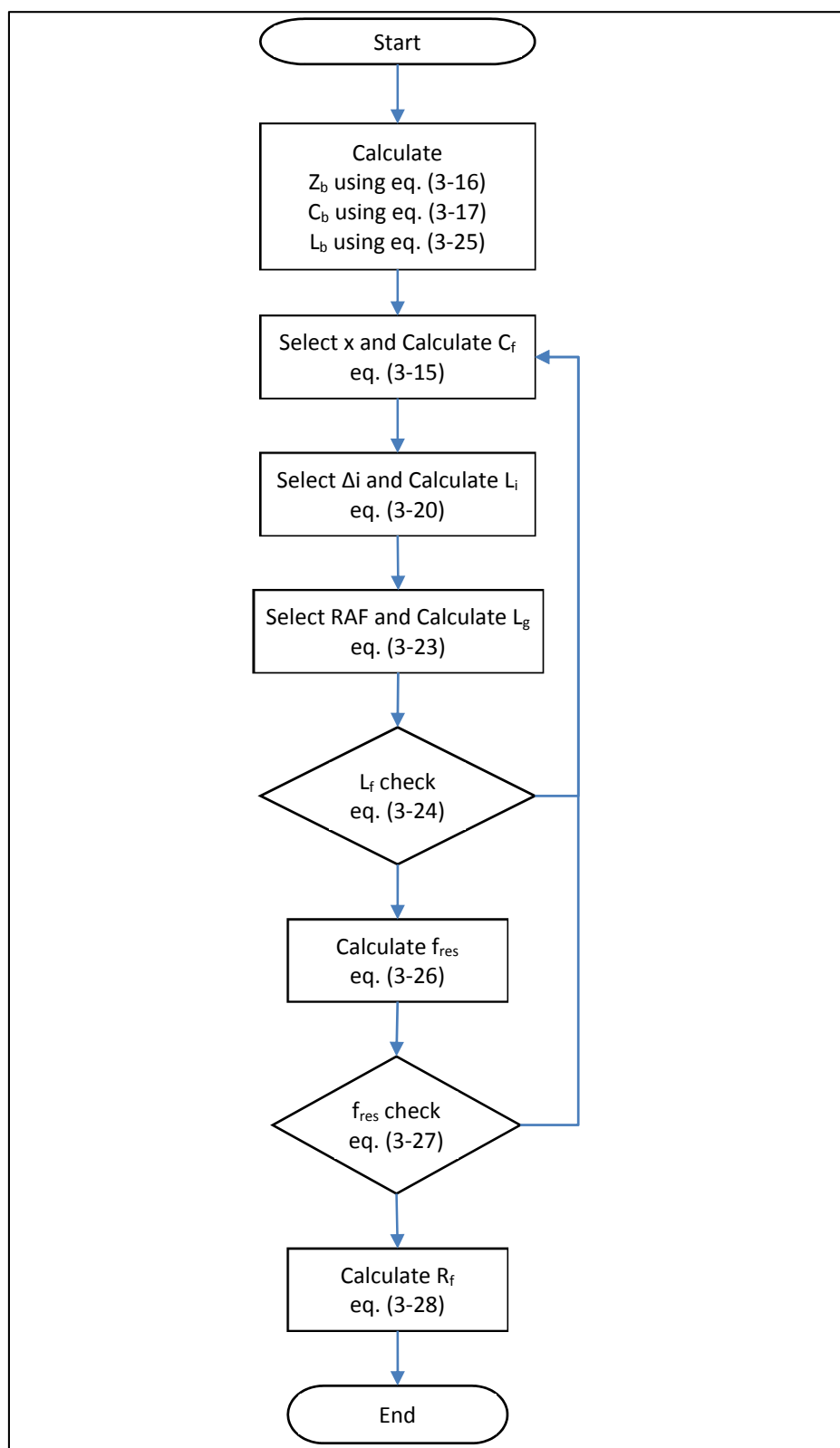
Figure 3-29 LCL-filter Design Flowchart

A SIMULINK circuit is built to test the LCL filter as shown in Figure 3-30. The VSI output current waveform and FFT spectrum without using a filter are shown in Figure 3-31. From the figure; it is obvious that the waveform has high the switching frequency harmonics. An LCL-filter is used to attenuate the high-frequency harmonics. The results are shown in Figure 3-32; the output current is almost sinusoidal with THD equal to 2% which is within the limits recommended by IEEE standards [38].
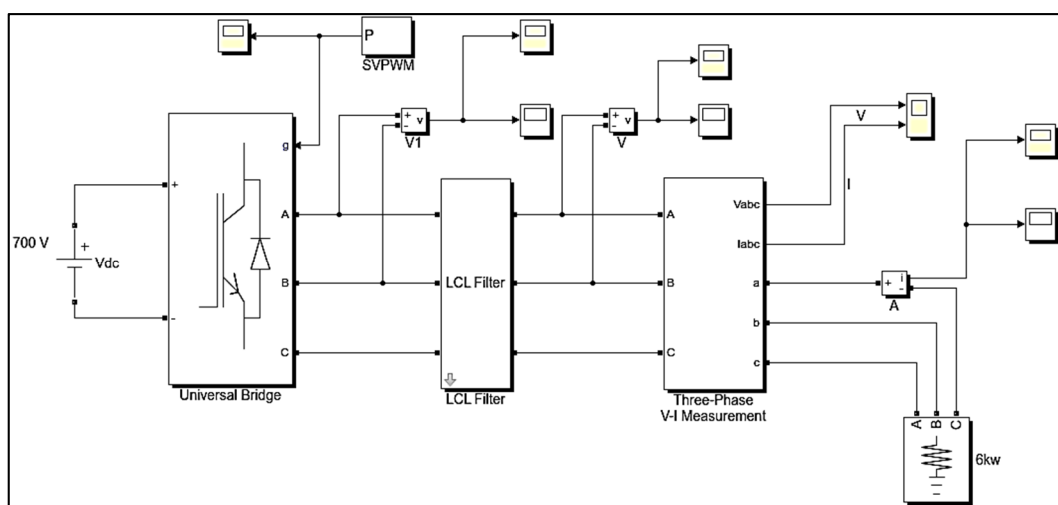
Figure 3-30 The SIMULINK Circuit for the Filter Test
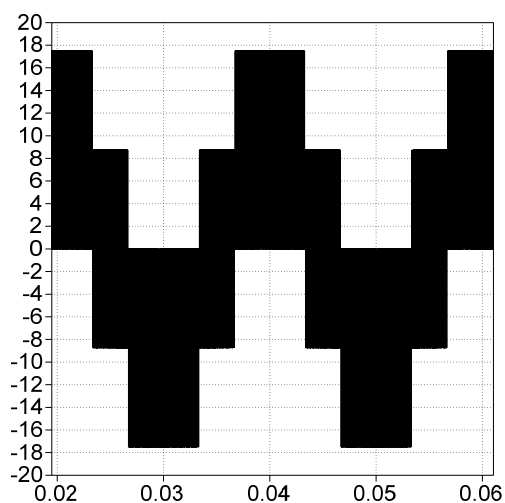
(a)
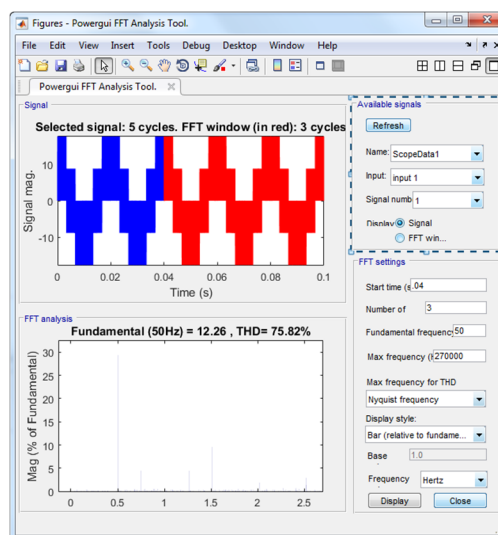
(b)

Figure 3-31 (a)The Output Current without Filtering (b)The Output Current FFT Spectrum

(a) (b)
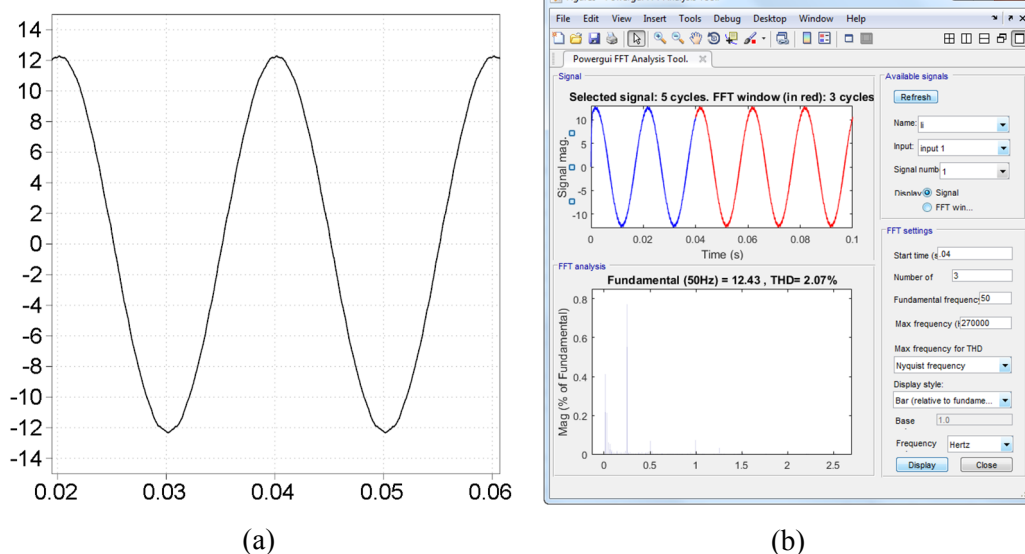
Figure 3-32 (a)The Output Current of the Inverter using LCL-filter (b)The Output Current FFT Spectrum

3.6 Phase Locked Loop (PLL)

The PLL is used to extract the phase of the grid voltage vector. The phase angle of the grid voltage is very important for control algorithms of grid-connected PV systems. It is used to control the inverter switches, calculate and control of active and reactive powers, and transform the feedback variables (grid voltage and current) to a reference frame suitable for control algorithms. The SIMULINK model for the PLL is shown in Figure 3-33.
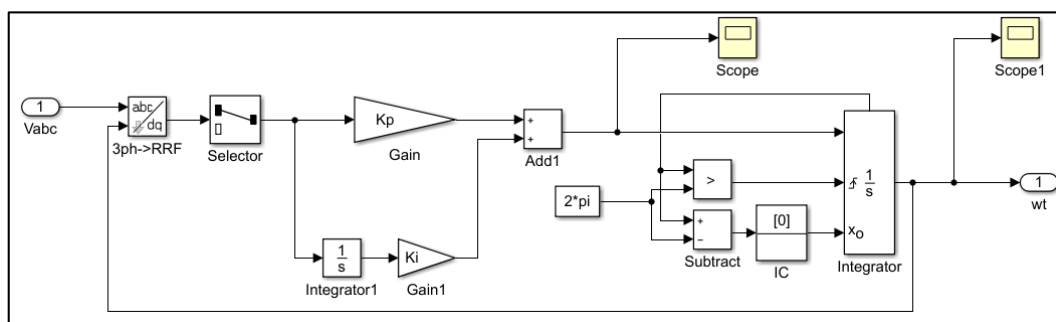
Figure 3-33 The SIMULINK Model for the PLL

The MATLAB circuit in Figure 3-34 was built to test the PLL. In this circuit, the PLL is used to detect the phase of a sine wave with a variable phase. The test results are shown in Figure 3-35. The first signal is the actual phase of the sine wave, the second signal is the detected phase using the PLL, and the final signal is the difference between the actual phase and measured one. From the result, it is clear that the measured phase is very close to the actual one.
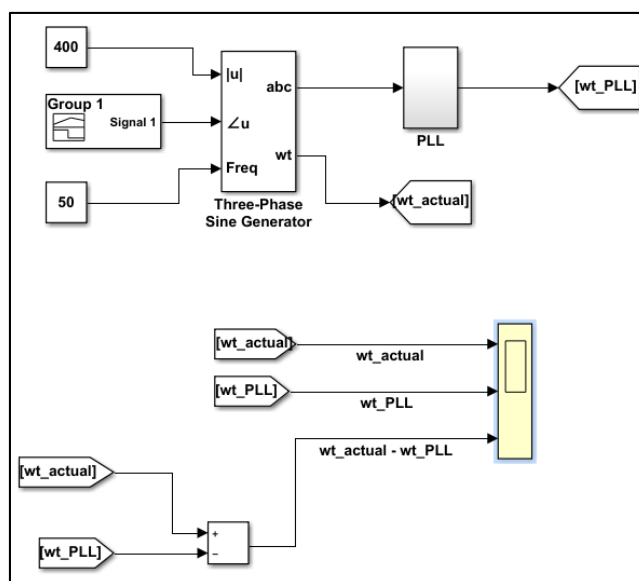
Figure 3-34 The MATLAB Circuit for the PLL Test
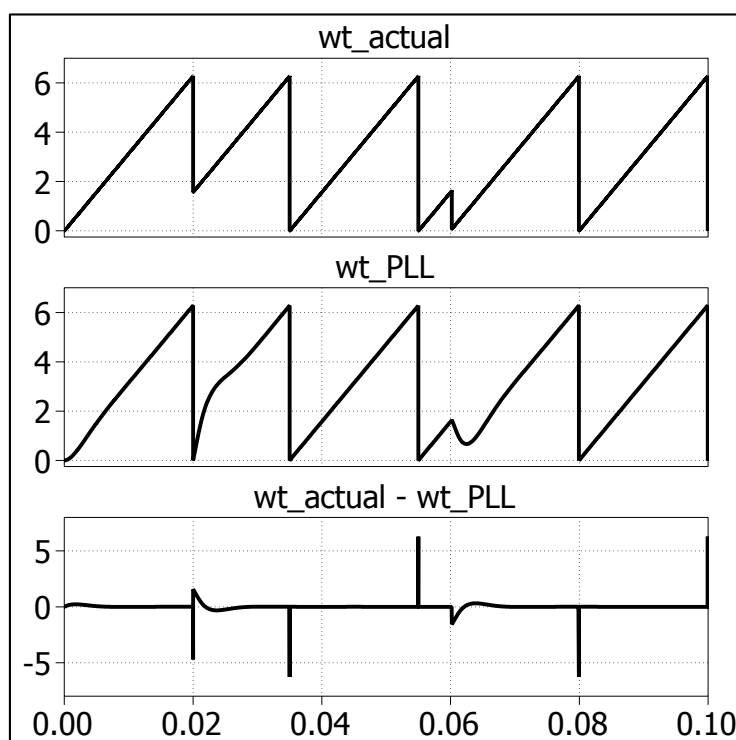
Figure 3-35 Test Results of the PLL

3.7 VSI Controller

The SIMULINK model for the VSI Controller shown in Figure 3-36. The controller tasks are achieved mainly by two loops: an external voltage loop, which adjusts the DC-link voltage, and internal current loop, which regulates the grid currents (I_d and I_q). The output of the active current (I_d*) reference is generated by the DC-link voltage controller. While

the reactive power controller sets the reactive current reference (I_q*). Using the phase angle of the grid voltages (Θ), the grid voltages and currents (V_{abc}, I_{abc}) are transformed into dq frame that rotates in synchronous with the grid voltage. Then, the current references are compared with the measured ones, and the error signals are fed into three current controllers. V_{di} and V_{qi} voltage outputs of the current controller are used as a reference to the SVPWM generator [12].

The grid-voltage and current transformation from abc to dq are shown in Figure 3-37. Figure 3-38 shows the generation of SVPWM to control the VSI.

Figure 3-36 The SIMULINK Model for the Active and Reactive Power Controller

Figure 3-37 The Grid Voltages and the Currents (abc to dq) Transformation
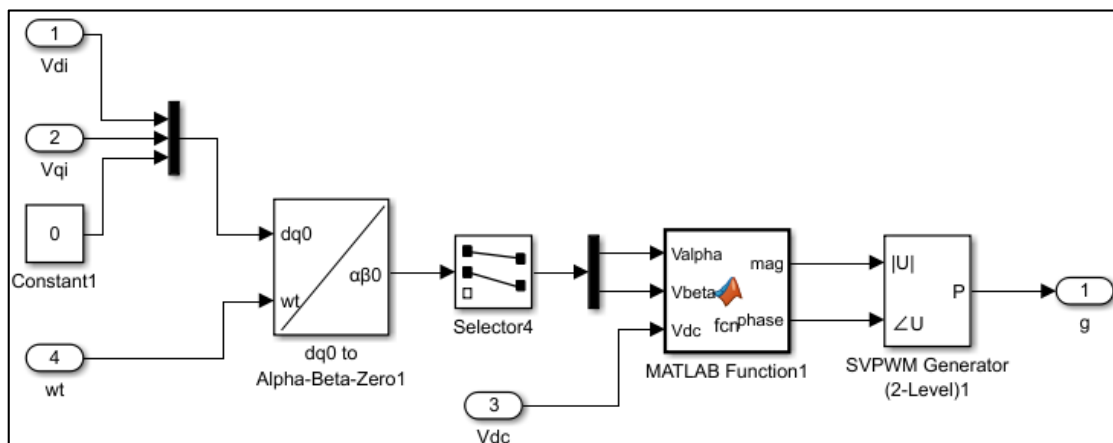
Figure 3-38 The SVPWM Generation

To test the active and reactive power controller, the circuit in Figure 3-39 was built. The DC voltage reference is set to 700 V, active power reference is set to 5kW and reactive power reference is set once to 0kVAR and then to 1kVAR. The simulation results (shown in Figure 3-40 and Figure 3-41) are matching the set values.
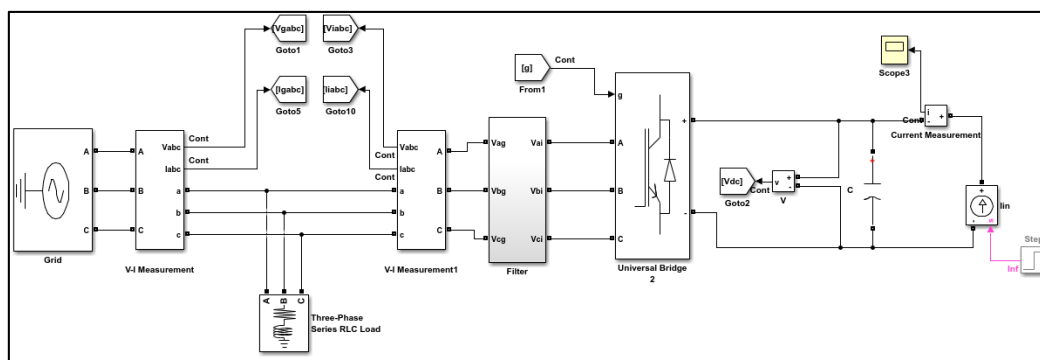
Figure 3-39 The Active and Reactive Power Controller Test Circuit
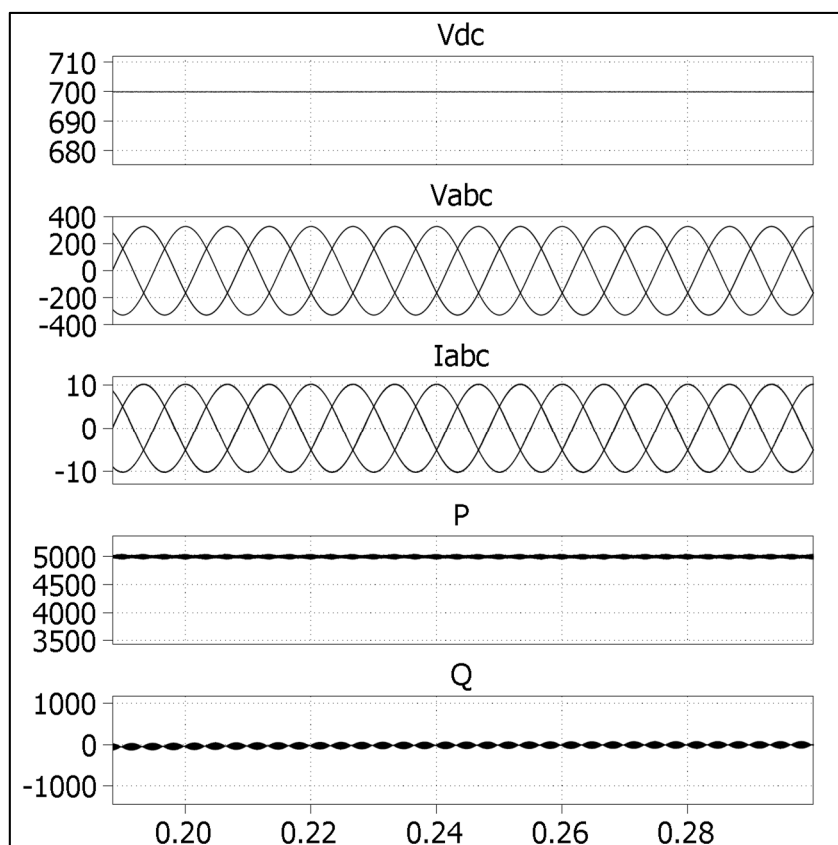
Figure 3-40 The simulation Results of the PQ Controller Test (Vdc=700V, P=5kW, Q=0kVAR)
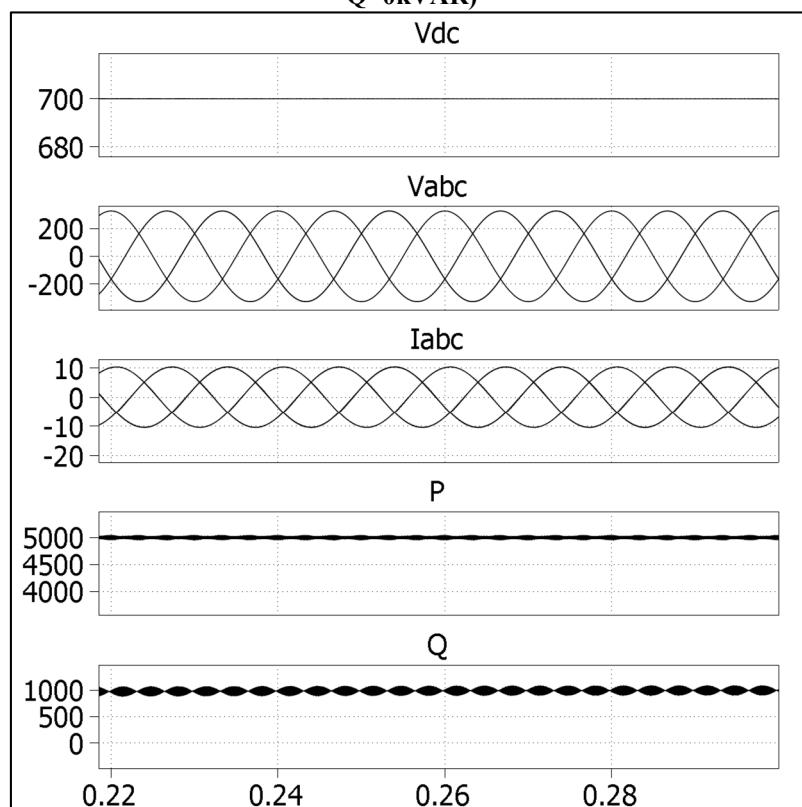
Figure 3-41 The Simulation Results of the PQ Controller Test (Vdc=700V, P=5kW, Q=1kVAR)

Chapter 4 THE GRID-CONNECTED PV SYSTEM

In Chapter 3, the main components of the grid-connected PV system have been modelled and tested. These components are the PV array, the DC-DC Boost converter, the VSI, the PLL, the LCL filter, the MPPT controller and the VSI controller. In this chapter, the entire grid-connected PV system will be built using the constructed components. The system will be tested under various weather and grid conditions, and the results will be analyzed and discussed.

The MATLAB/SIMULINK model for the grid-connected PV system is shown in Figure 4-1. The description of the model is as follows:

The PV Array: The PV array consists of two parallel strings. Each string has 15 Kyocera KC200GT solar modules [59] connected in series. The PV array is generating a maximum power of 6kW at STC (1000 W/m^2 sun irradiance and 25°C temperature).

The DC-DC Boost Converter: a Boost converter used to step-up the PV array MPP output voltage (V$_{MPP}$) from 395V at STC to 700V. The Boost converter is operated at a switching frequency of 10 kHz. The duty cycle of the Boost converter is generated by the MPPT controller.

The MPPT Controller: uses the Perturb and Observe (P&O) technique to generate the duty cycle of the Boost converter. This controller automatically varies the duty cycle of the boost converter in order to extract the maximum power from the PV array.

The VSI: a 3-level IGBT VSI inverter is used to convert the 700V DC-link voltage to 400V$_{LLrms}$ AC voltage. The inverter switches are controlled using SVPWM technique. The SVPWM signals are generated by the inverter controller.

VSI controller (described in Section 3.7): it is used to generate the appropriate gate signals for the VSI switches in order to generate the required AC voltages and currents.

Grid filter: an LCL filter is used to filter harmonics produced by VSI.

The grid: the PV array is connected to 400V$_{LLrms}$ grid line.

The local load: the PV array is supplying a 4kW local load; the extra inverter power is supplied to the grid.
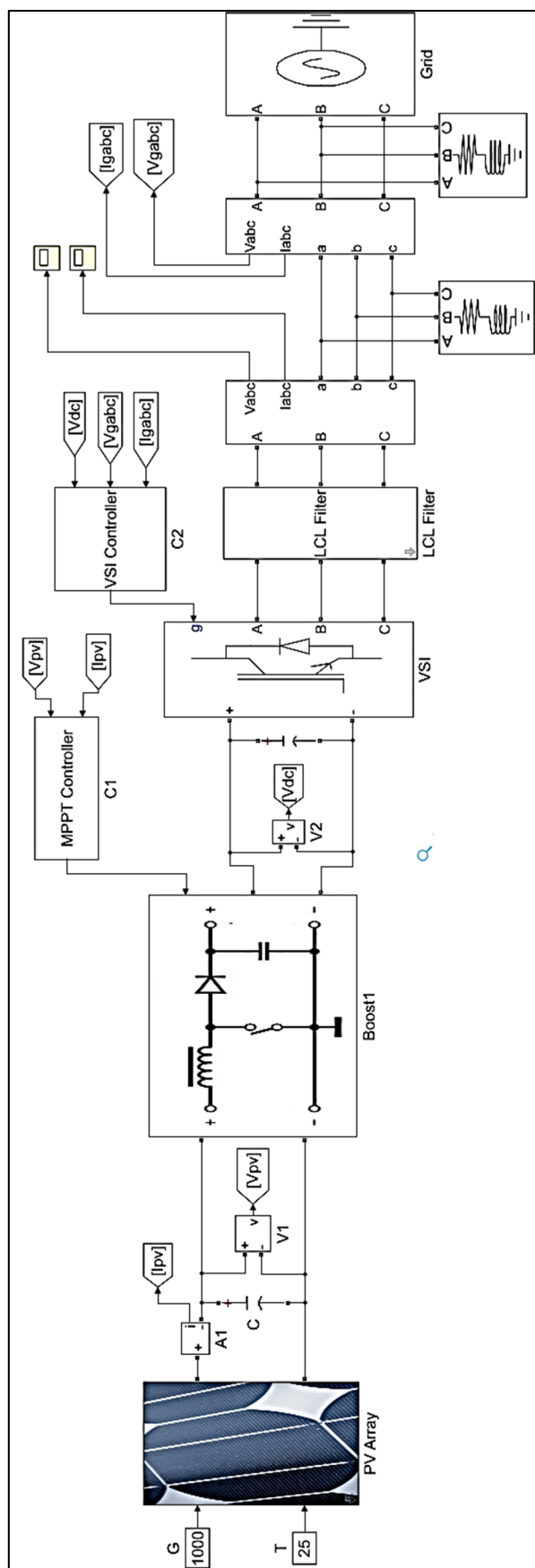
Figure 4-1 MATLAB Model for the Grid-Connected PV System

4.1 Grid-Connected PV System under STC

The first test is conducted by applying 1000 W/m² sun irradiance and 25°C temperature to the PV array. The simulation results are shown in Figure 4-2. From the figure, it is possible to conclude the followings:

- The DC-link voltage is equal to the set value (700 V DC)
- The output phase voltage from VSI is synchronized with grid voltage (same magnitude, frequency, and phase angle)
- The output power for the inverter equals 5760 Watt, which means that the inverter has 96% efficiency (the PV array power is 6kW) Figure 4-3 shows the inverter output current and voltage before and after the filtration. The inverter current has a small THD (less than 2%) as shown in Figure 4-4 .
- The reactive power equals zero. (No reactive load)
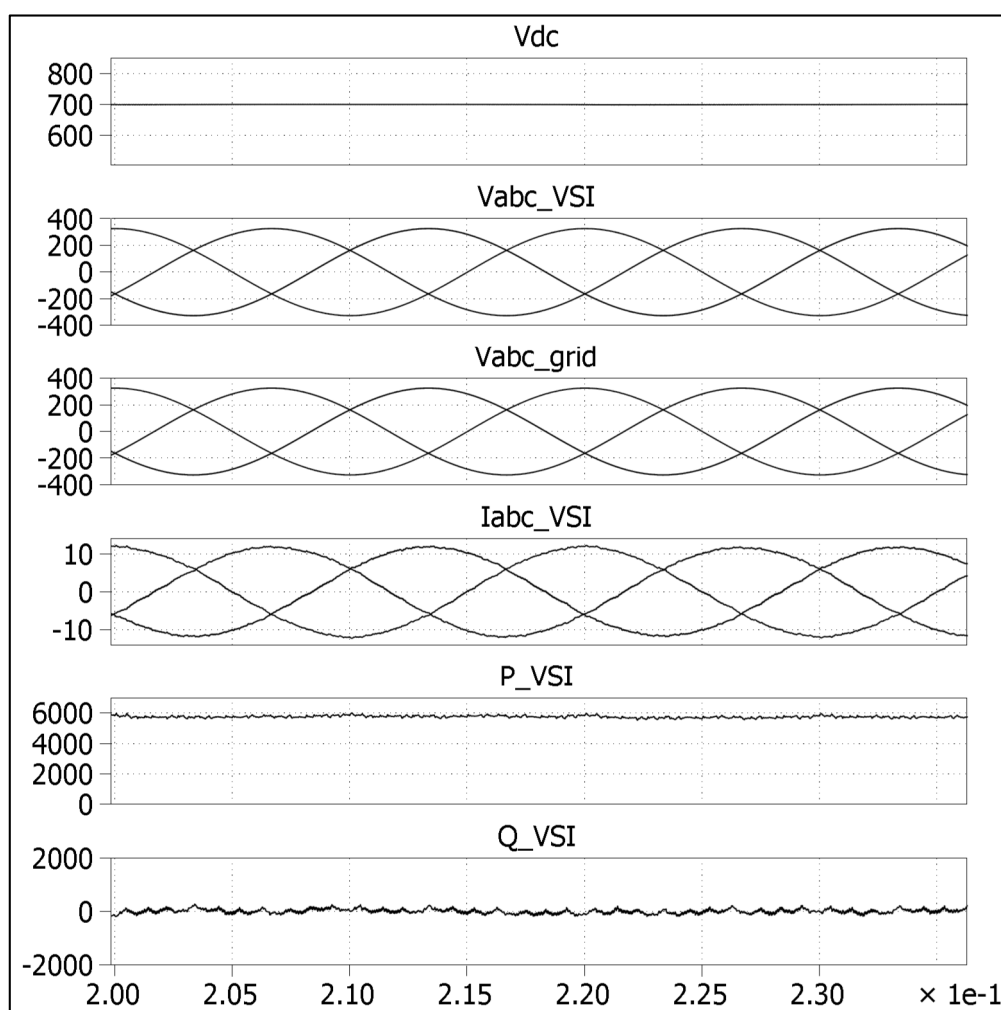
Figure 4-2: Outputs of the Grid-connected PV System Test at STC
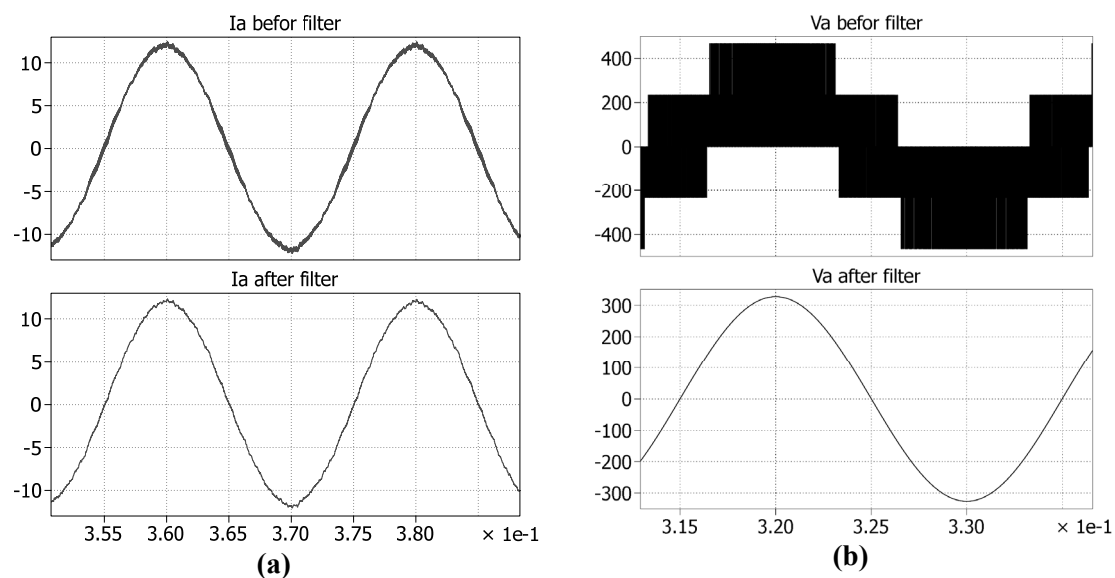
Figure 4-3 The Unfiltered and Filtered Outputs of the Inverter (a) Current Waveforms (b) Voltage Waveforms
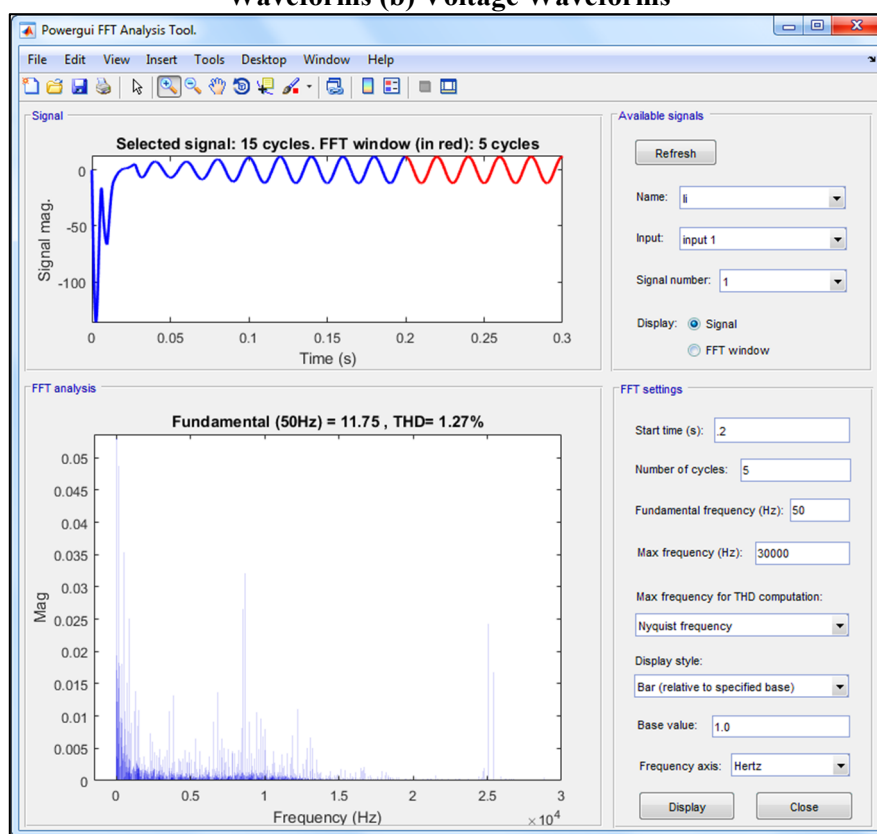
Figure 4-4 FFT Analysis of the Inverter Output Current

4.2 Grid-Connected PV System under Various Temperatures and Irradiance Levels

The second test is done by applying a variable irradiance and temperature to the PV array. The simulation results are shown in Figure 4-5. From the Figure; it is possible to conclude the following:

- The DC-link voltage remains constant and equals the set value (700 V DC)
- The output voltage from the VSI is synchronized with the grid voltage (same magnitude, frequency, and phase).
- The magnitude and the phase of the inverter current vary according to the active power supplied by the PV array.
- The PV array output power and the inverter output power are summarized in Table 4-1
- Figure 4-6 illustrates the operation of the MPPT controller. It shows the output power from the PV array versus the PV array voltage.

Table 4-1 Summarization of the MPPT Test Results

Irradiance (W/m^2)	Temperature (°C)	PV Power (W)	Inverter Power (W)
400	25	2192	1947
800	25	4706	4453
1000	25	6010	5760
1000	10	6464	6218
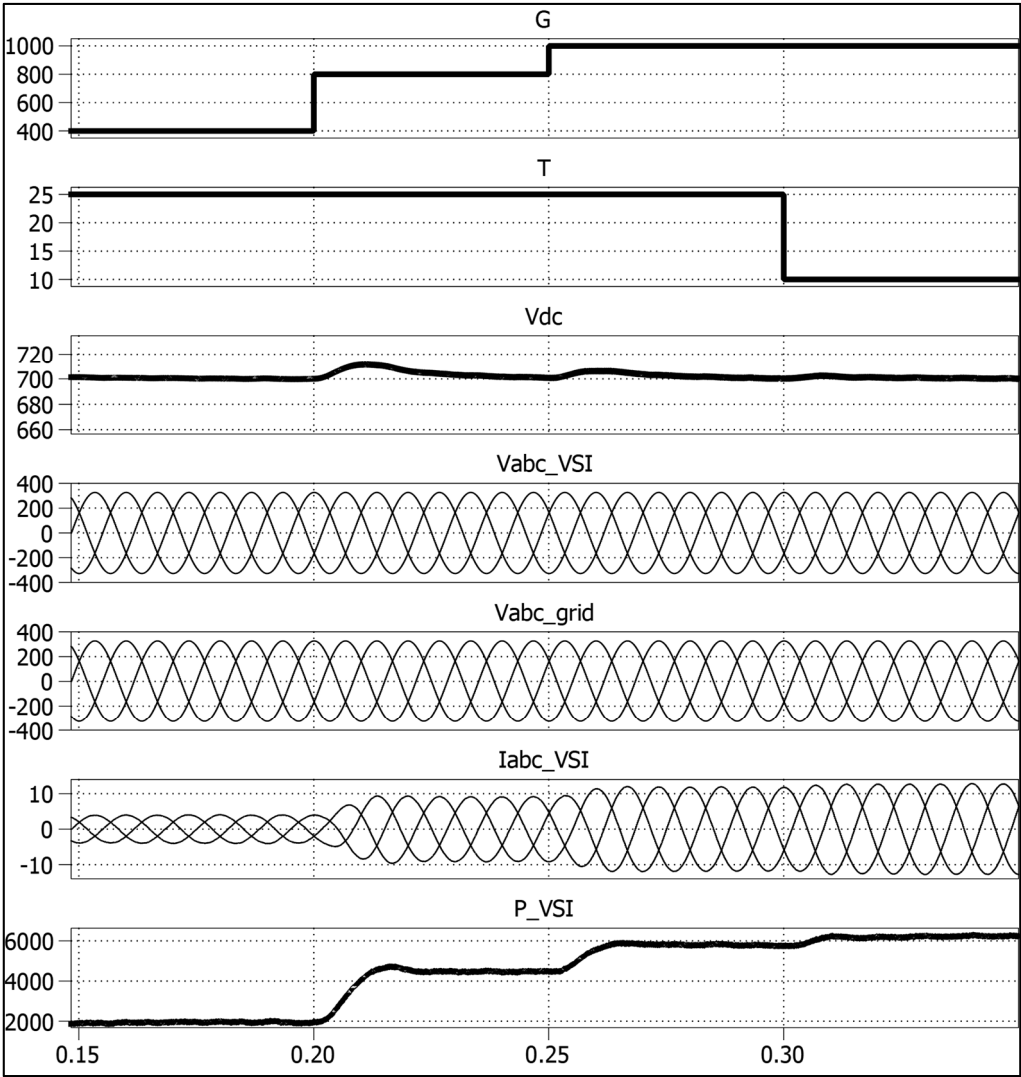
Figure 4-5 Grid-Connected PV System Test under Various Temperatures and Irradiance Levels
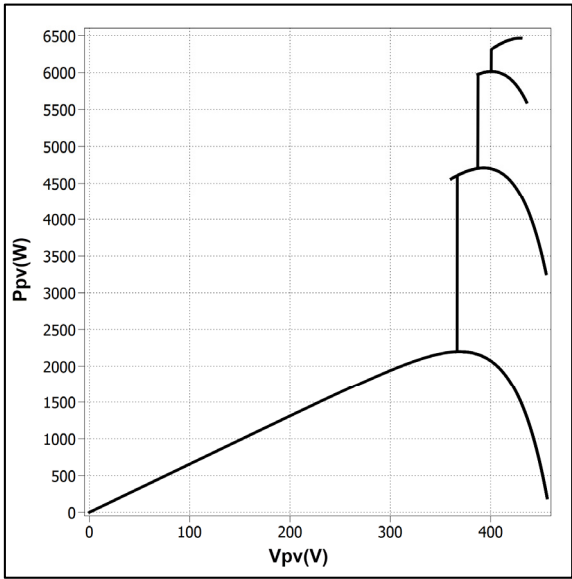
Figure 4-6 PV Array Output Power vs. Output Voltage

4.3 Grid-Connected PV System Supplying Reactive Load

In this test, the PV array is working under STC and supplying an 8kW/500VAR local load. The inverter voltage, current, active power, and reactive power are shown in Figure 4-7. The voltage, current, active power and reactive power of the grid are shown in Figure 4-8. From the Figures, it is possible to observe the following:

- The active power sharing between the PV array and the grid. The PV array is supplying its maximum power to the load (about 6kW), while the grid is supplying the remaining power required by the load (2kW).

- The PV array is supplying the full reactive power required by the load (500VAR), while the grid is working on unity power factor (supplying zero reactive power).
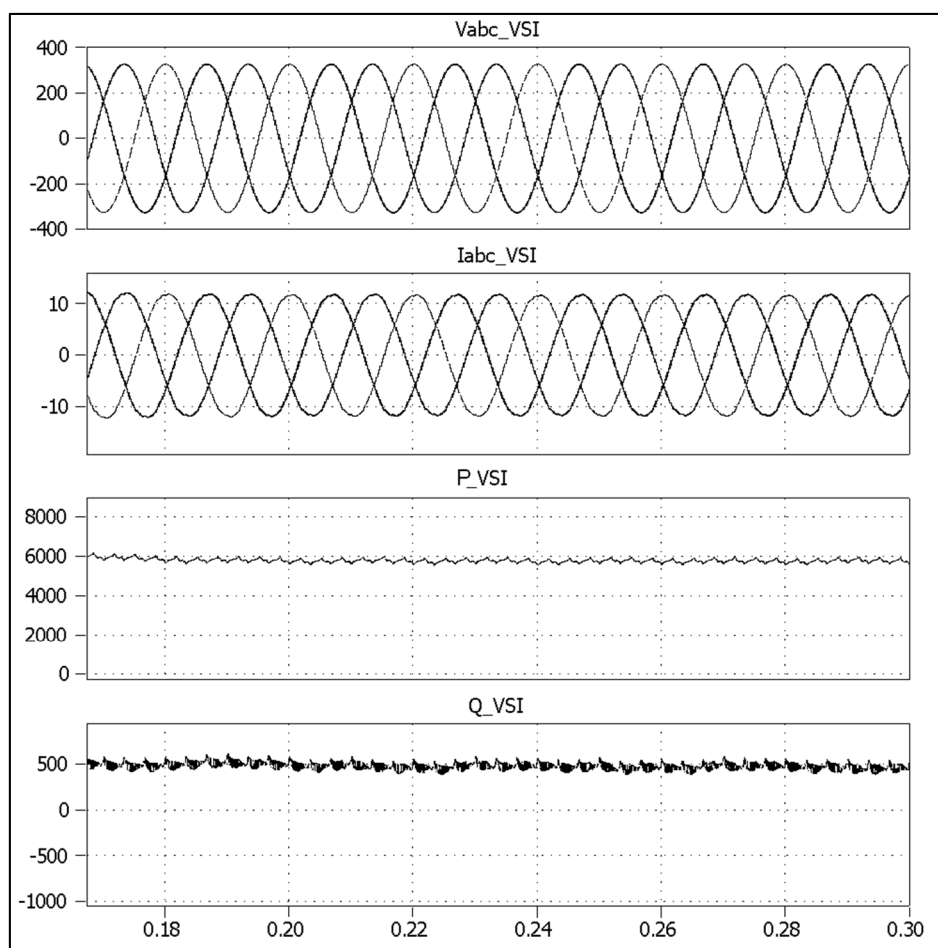
Figure 4-7 Inverter Voltage, Current, Active Power, and Reactive Power
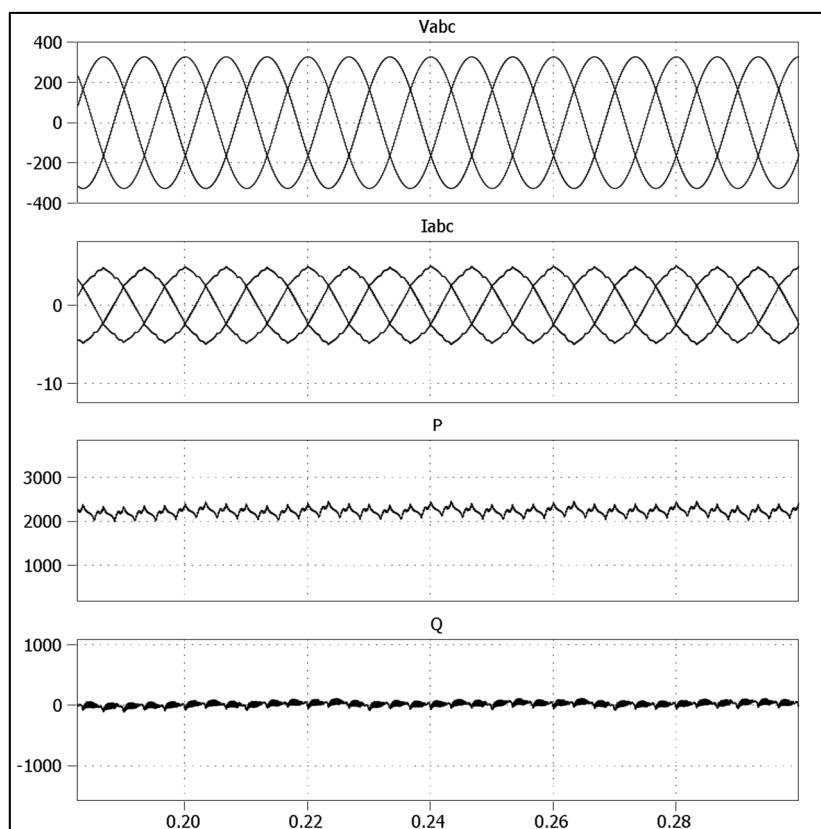
Figure 4-8 Grid Voltage, Current, Active Power, and Reactive Power

4.4 Grid-Connected PV System Working Overnight

In this test, the PV array is working overnight, which means that it is supplying zero active power. The PV array is connected to a 3kW/500VAR local load. The inverter voltage, current, active power, and reactive power are shown in Figure 4-9. The voltage, current, active power and reactive power of the grid are shown in Figure 4-10. From the Figures, it is possible to observe the following:

- The PV array is supplying zero active power. However, it still can supply all the reactive power required by the load (500VAR).
- The inverter is controlled to ensure that the grid is working at a unity power factor. It is obvious that the grid is supplying all the active power required by the load (3kW) and it is supplying zero reactive power.
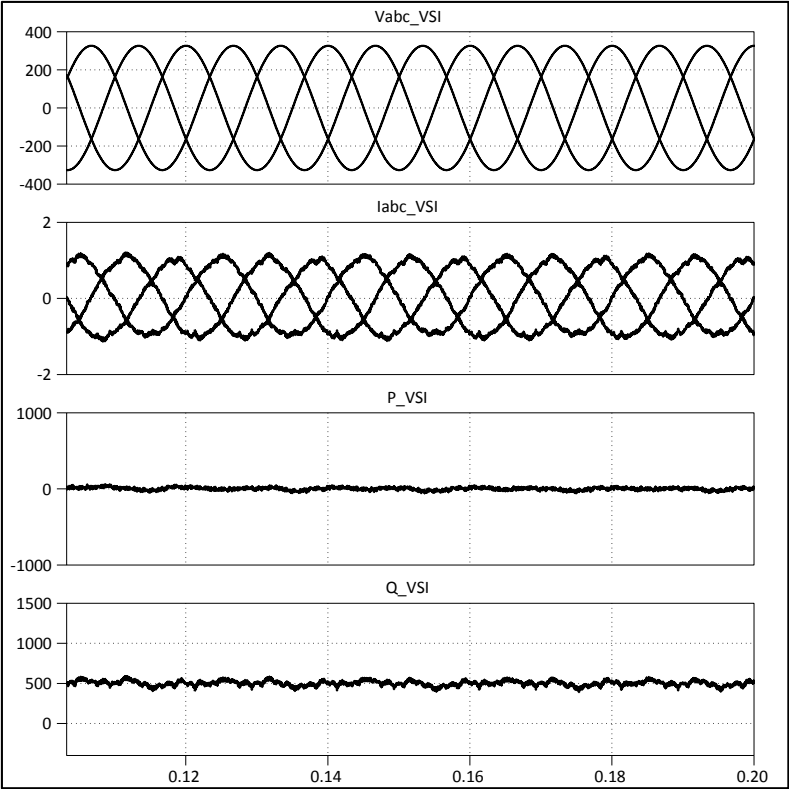
Figure 4-9 Inverter Voltage, Current, Active Power, and Reactive Power
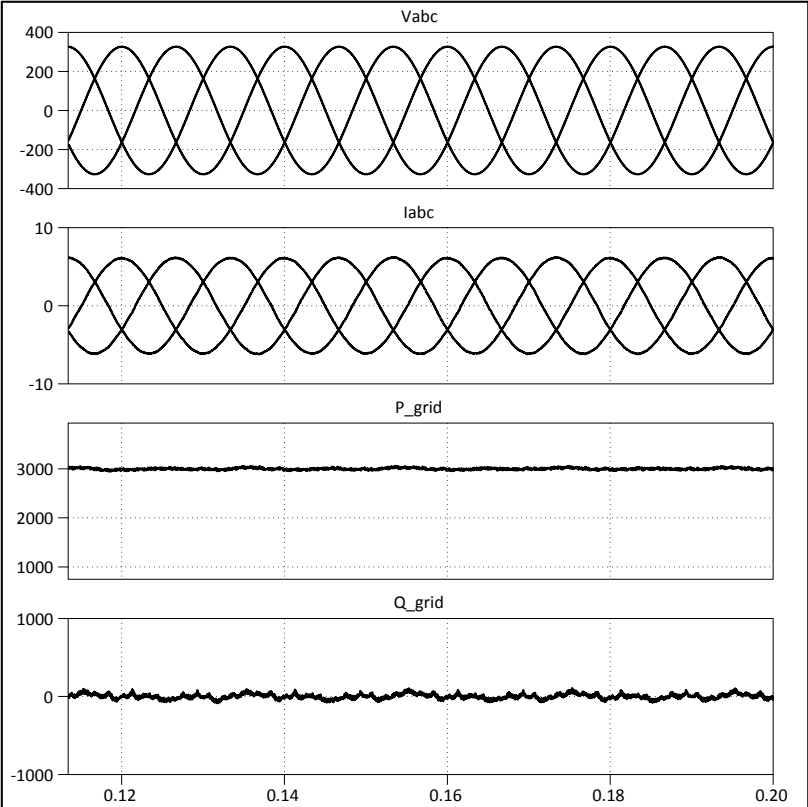
Figure 4-10 Grid Voltage, Current, Active Power, and Reactive Power

Chapter 5   CONCLUSIONS AND FUTURE WORK

5.1 *Conclusions*

In this thesis, a comprehensive literature review has been presented to identify the most efficient and reliable hardware structures, and control algorithms for a grid-connected PV system. The hardware structure is mainly based on three devices: the DC-DC Boost converter, the inverter, and LCL-filter.

Many control and protection algorithms have been proposed in the literature to maximize the PV output power and protect the system. The most important ones are the MPPT, active and reactive power control, DC-link control, harmonic elimination, synchronization, and islanding protection.

The problem to be addressed by this thesis is how to build a high efficient grid-connected PV system and to develop advanced control and synchronization algorithms, which would improve the efficiency, stability, and reliability of the grid-connected PV system under normal and fault conditions.

To achieve this, the whole PV system should be tested under the variable weather and grid conditions. However, the wide variety of devices and control algorithms makes the practical testing of the system very difficult and expensive. Moreover, in real systems, many types of scenarios and faults cannot be studied due to the destructive nature they may cause to the system. Therefore, this thesis makes use of the modelling and simulation tools of MATLAB/ SIMULINK to develop a grid-connected PV model that can be used to simulate any scenario or fault, which enables setting the appropriate control and protection scheme.

The modelling tasks and control algorithms have been done and presented in Chapter 3. An accurate model for PV array was built using MATLAB/SIMULINK. The accuracy of the model was verified by comparing the results with the datasheet information. Then, the DC-DC Boost converter was designed and used to step-up the output voltage of the PV array to a suitable level. Moreover, The Perturb and Observe (P&O) MPPT control technique was implemented and used to extract the maximum power from the PV array. In addition, a Three-phase Voltage Inverter (VSI) was modelled and controlled using SVPWM to

convert the DC voltage to an AC voltage synchronized with the grid voltage. An LCL-filter was designed and used to attenuate the high-frequency harmonics at the output of the inverter. Finally, a DC-link controller and active and reactive power controller were implemented and tested.

Finally, a model for a grid-connected PV system was built and tested under various weather and grid conditions. In the first test, the model was tested under STC to show how the PV array system is synchronized with the utility grid to supply its maximum power. The second test was done under various temperatures and irradiance levels, which shows how the MPPT controller succeeded in extracting the maximum power from the PV array. Next, an 8kW/500VAR local load was connected to the system under STC. This test demonstrated the power sharing between the PV array and the grid. In the final test, the system was tested overnight. In this test, the PV array system acted as a reactive power compensator; it supplied all reactive power required by the local load and ensured that the grid works at a unity power factor.

At the end of this thesis, it can be argued that the desired model for the grid-connected PV system has been successfully constructed. The tests results showed that the system operates efficiently and effectively under various grid and weather conditions. Consequently, the constructed model can be used to perform further studies and researches on the grid-connected PV system and its components, which will help in developing more efficient and advanced hardware structures, control algorithms, and protection schemes.

5.2 Future Work

- Perform some practical experiments to verify the simulation results.

- Using the developed model to construct comparative studies on different control algorithms and hardware structures.

- Using the constructed model to perform a fault analysis study on the system.

REFERENCES

[1]   R. Fu *et al.*, "U.S. Solar Photovoltaic System Cost Benchmark: Q1 2016," 2016.

[2]   IEA-PVPS, "2016 Snapshot of global photovoltaic markets," 2016.

[3]   IRENA, "Renewable capacity statistics 2017," 2017.

[4]   REN21 Secretariat, "Renewables 2017 global status report," 2017.

[5]   A. Jäger-Waldau, "PV status report 2016," 2016.

[6]   M. Rashid, *Power electronics handbook*, 3rd ed. Elsevier, 2011.

[7]   REN 21 Steering Committee, "Renewables 2013 global status report." 2013.

[8]   G. M. Masters, *Renewable and Efficient Electric Power Systems*. Hoboken, NJ, USA: John Wiley & Sons, Inc., 2004.

[9]   R. Singh and B. S. Rajpurohit, "Performance Evaluation of Grid-Connected Solar Photovoltaic (SPV) System with Different MPPT Controllers," 2014, pp. 97–124.

[10]   G. J. Kish *et al.*, "Modelling and control of photovoltaic panels utilising the incremental conductance method for maximum power point tracking," *IET Renewable Power Generation*, vol. 6, no. 4. p. 259, 2012.

[11]   M. L. and P. R. Remus Teodorescu, *Grid Converters for Photovoltaic and Wind Power Systems*. 2011.

[12]   F. Blaabjerg *et al.*, "Overview of Control and Grid Synchronization for Distributed Power Generation Systems," *IEEE Transactions on Industrial Electronics*, vol. 53, no. 5. pp. 1398–1409, 2006.

[13]   samlexsolar, "Solar PV Cell Module, array." .

[14]   B. Parida *et al.*, "A review of solar photovoltaic technologies," *Renewable and Sustainable Energy Reviews*, vol. 15, no. 3. pp. 1625–1636, Apr. 2011.

[15]   IRENA, "Renewable energy technologies: Cost analysis series," *Concentrating solar power*. 2012.

[16]   M. A. Green *et al.*, "Solar cell efficiency tables (version 49)," *Progress in Photovoltaics: Research and Applications*, vol. 25, no. 1. pp. 3–13, Jan. 2017.

[17]   M. G. G. Villalva *et al.*, "Comprehensive Approach to Modeling and Simulation of Photovoltaic Arrays," *IEEE Transactions on Power Electronics*, vol. 24, no. 5. pp. 1198–1208, May 2009.

[18]   H.-L. Tsai *et al.*, "Development of Generalized Photovoltaic Model Using MATLAB/SIMULINK," in *World Congress on Engineering and Computer Science*, 2008, pp. 0–5.

[19]   Y. Mahmoud *et al.*, "A Simple Approach to Modeling and Simulation of Photovoltaic Modules," *IEEE Transactions on Sustainable Energy*, vol. 3, no. 1. pp. 185–186, Jan. 2012.

[20]   S. Bal *et al.*, "Comparative analysis of mathematical modeling of Photo-Voltaic (PV) array," in *Annual IEEE India Conference (INDICON*, 2012, pp. 269–274.

[21]   J. a. Gow and C. D. Manning, "Development of a photovoltaic array model for use in power-electronics simulation studies," *IEE Proceedings - Electric Power Applications*, vol. 146, no. 2. p. 193, 1999.

[22]   E. Romero-Cadaval *et al.*, "Grid-Connected Photovoltaic Generation Plants: Components and Operation," *IEEE Industrial Electronics Magazine*, vol. 7, no. 3. pp. 6–20, Sep. 2013.

[23]   T. Esram and P. L. Chapman, "Comparison of Photovoltaic Array Maximum Power Point Tracking Techniques," *IEEE Transactions on Energy Conversion*, vol. 22, no. 2. pp. 439–449, 2007.

[24]   M. A. G. de Brito *et al.*, "Evaluation of the main MPPT techniques for photovoltaic applications," *IEEE Transactions on Industrial Electronics*, vol. 60, no. 3. pp. 1156–1167, Mar. 2013.

[25]   D. Sera *et al.*, "On the Perturb-and-Observe and Incremental Conductance MPPT Methods for PV Systems," *IEEE Journal of Photovoltaics*, vol. 3, no. 3. pp. 1070–1078, Jul. 2013.

[26]   S. E. Babaa *et al.*, "Overview of Maximum Power Point Tracking Control Methods for PV Systems," *Journal of Power and Energy Engineering*, vol. 2, no. 8. Scientific Research Publishing, pp. 59–72, 2014.

[27]   K. H. Hussein *et al.*, "Maximum photovoltaic power tracking: an algorithm for rapidly changing atmospheric conditions," *IEE Proceedings-Generation, Transmission and Distribution*, vol. 142, no. 1. IET, pp. 59–64, 1995.

[28]   G. Walker, "Evaluating MPPT converter topologies using a MATLAB PV model," *Journal of Electrical & Electronics Engineering*, vol. 21, no. 1. Engineers Australia, p. 49, 2001.

[29]   M. Rashid, *Power Electronics: Circuits, Devices, and Applications*, 3rd ed. Prentice Hall, 2003.

[30]   N. Mohan *et al.*, *Power Electronics: Converters, Applications and Design*, 3rd ed. John Wiley & Sons, Ltd, 2003.

[31]   P. P. Krause *et al.*, *Analysis of electric machinery and drive systems*, 3rd ed. Wiley, 2013.

[32]   A. Timbus, "Grid monitoring and advanced control of distributed power generation systems," Aalborg University, 2007.

[33]   A. Timbus *et al.*, "Synchronization methods for three phase distributed power generation systems - An overview and evaluation," *IEEE 36th Power Electronics Specialists Conference*. pp. 2474–2481, 2005.

[34]   A. Nagliero *et al.*, "Monitoring and synchronization techniques for single-phase {PV} systems," *International Symposium on Power Electronics Electrical Drives Automation and Motion (SPEEDAM)*. Ieee, pp. 1404–1409, 2010.

[35]   Y. Yang and F. Blaabjerg, "Overview of Single-phase Grid-connected Photovoltaic Systems," *Electric Power Components and Systems*, vol. 43, no. 12. Taylor & Francis, pp. 1352–1363, Jul. 2015.

[36]   G. Hsieh and J. Hung, "Phase-locked loop techniques. A survey," *IEEE Transactions on Industrial Electronics*. 1996.

[37]   M. Boyra and J.-L. Thomas, "A review on synchronization methods for grid-connected three-phase VSC under unbalanced and distorted conditions," in *European Conference on Power Electronics and Applications*, 2011, pp. 1–10.

[38]   "IEEE Standard for Interconnecting Distributed Resources with Electric Power Systems," 2003.

[39]   "Photovoltaic (PV) systems – Characteristics of the utility interface." 2004.

[40]   "Automatic Disconnection Device between a Generator and the Public Low-Voltage Grid, VDE V 0126-1-1 Std., 2006." 2006.

[41]   F. De Mango *et al.*, "Overview of Anti-Islanding Algorithms for PV Systems. Part I: Passive Methods," *12th International Power Electronics and Motion Control Conference*. pp. 1878–1883, 2006.

[42]   F. De Mango *et al.*, "Overview of Anti-Islanding Algorithms for PV Systems. Part II: Active Methods," *12th International Power Electronics and Motion Control Conference*. pp. 1884–1889, 2006.

[43]   W. W. Y. Teoh and C. W. C. Tan, "An Overview of Islanding Detection Methods in Photovoltaic Systems," *World Academy of Science, Engineering and Technology*, vol. 5, no. 58. pp. 674–682, 2011.

[44]   D. Velasco *et al.*, "Review of anti-islanding techniques in distributed generators," *Renewable and Sustainable Energy Reviews*, vol. 14, no. 14. pp. 1608–1614, Aug. 2010.

[45]   F. Blaabjerg *et al.*, "Power Electronics for Renewable Energy Systems – Status and Trends," *8th International Conference on Integrated Power Systems (CIPS)*. pp. 25–27, 2014.

[46]   J. M. M. Carrasco *et al.*, "Power-Electronic Systems for the Grid Integration of Renewable Energy Sources: A Survey," *IEEE Transactions on Industrial Electronics*, vol. 53, no. 4. pp. 1002–1016, Jun. 2006.

[47]   R. H. H. Lasseter, "MicroGrids," in *IEEE Power Engineering Society Winter Meeting, 2002.*, 2002, vol. 1, pp. 305–308 vol.1.

[48]   Blaabjerg *et al.*, "Power electronics as efficient interface in dispersed power generation systems," *IEEE Transactions on Power Electronics*, vol. 19, no. 5. IEEE, pp. 1184–1194, 2004.

[49]   F. Blaabjerg and F. Iov, "Power electronics-key technology for renewable energy systems," *Power Electronics, Drive Systems and Technologies Conference (PEDSTC)*. pp. 445–466, 2011.

[50]   S. B. Kjaer *et al.*, "A review of single-phase grid-connected inverters for photovoltaic modules," *IEEE Transactions on Industrial Electronics*, vol. 41, no. 5. pp. 1292–1306, 2005.

[51]   T. Orłowska-Kowalska *et al.*, *Advanced and Intelligent Control in Power Electronics and Drives*, vol. 531. Cham: Springer, 2014.

[52] D. Meneses *et al.*, "Review and comparison of step-up transformerless topologies for photovoltaic AC-module application," *IEEE Transactions on Power Electronics*, vol. 28, no. 6. pp. 2649–2663, 2013.

[53] F. Luo and H. Ye, *Advanced DC/AC Inverters: Applications in Renewable Energy.* CRC Press, 2013.

[54] T. Kerekes *et al.*, "A New High-Efficiency Single-Phase Transformerless PV Inverter Topology," *IEEE Transactions on Industrial Electronics*, vol. 58, no. 1. pp. 184–191, 2011.

[55] L. G. Franquelo *et al.*, "The age of multilevel converters arrives," *IEEE Industrial Electronics Magazine*, vol. 2, no. 2. pp. 28–39, 2008.

[56] M.-Y. Park *et al.*, "LCL-filter design for grid-connected PCS using total harmonic distortion and ripple attenuation factor," *The 2010 International Power Electronics Conference - ECCE ASIA -*. Ieee, pp. 1688–1694, Jun. 2010.

[57] H. Cha and T. Vu, "Comparative analysis of low-pass output filter for single-phase grid-connected Photovoltaic inverter," in *2010 Twenty-Fifth Annual IEEE Applied Power Electronics Conference and Exposition (APEC)*, 2010, pp. 1659–1665.

[58] J. Lettl *et al.*, "Comparison of different filter types for grid connected inverter," *PIERS Proceedings*. 2011.

[59] Kyocera, "KC200GT High Efficiency Multicrystal Photovoltaic Module Datasheet." .

[60] G. Spagnuolo *et al.*, "Efficient Approaches for Modeling and Simulating Photovoltaic Power Systems," *Photovoltaics, IEEE ...*, vol. 3, no. 1. pp. 500–508, 2013.

[61] B. M. Hasaneen and A. A. E. Mohammad, "Design and Simulation of DC/DC Boost Converter," *12th International Middle-East Power System Conference*. pp. 335–340, 2008.

[62] R. Zaitsu, "Voltage Mode Boost Converter Small Signal Control Loop Analysis Using TPS61030," 2009.

[63] K. Zhou and D. Wang, "Relationship between space-vector modulation and three-phase carrier-based PWM: a comprehensive analysis [three-phase inverters]," *IEEE Transactions on Industrial Electronics*, vol. 49, no. 1. pp. 186–196, 2002.

[64] W.-F. Zhang *et al.*, "Comparison of Three SVPWM Strategies," *Journal of Electronic Science and Technology*, vol. 5, no. 3. Editorial Board of Journal of University of Electronic Science and Technology, pp. 283–287, 2007.

[65] X. Wei *et al.*, "Design of LCL filter for wind power inverter," in *2010 World Non-Grid-Connected Wind Power and Energy Conference*, 2010, pp. 1–6.

[66] T. C. T. C. Y. Wang *et al.*, "Output filter design for a grid-interconnected three-phase inverter," in *IEEE 34th Annual Conference on Power Electronics Specialist*, 2003, vol. 2, pp. 779–784.

[67] L. M. *et al.*, "Design and control of an LCL-filter-based three-phase active rectifier," *IEEE Transactions on Industry Applications*, vol. 41, no. 5. pp. 1281–1291, Sep. 2005.

[68] M. Liserre *et al.*, "Design and control of an LCL-filter-based three-phase active rectifier," *IEEE Transactions on Industry Applications*, vol. 41, no. 5. pp. 1281–1291, 2005.

Appendix A   MATLAB CODES

A.1   MATLAB code to get the PV characteristic curves

```
open_system('PVArray2')
S=1;
P=1;
Rsh=1e5;
Voc=35;
Isc=8.5;
Pmax=205;
Temp=25;
for (G=200:200:1000)
sim('PVArray2')
v = V.signals.values;
i= I.signals.values;
p=v.*i;
[pmax,I] = max(p)
figure(1);
hold all
plot (v,i,'DisplayName',['T=' num2str(Temp) '^{\o}C, G=' num2str(G) 'W/m{^2}'])
plot(v(I),i(I),'r.','MarkerSize',20,'HandleVisibility','off');
figure(2);
hold all
plot (v,p,'DisplayName',['T=' num2str(Temp) '^{\o}C, G=' num2str(G) 'W/m{^2}'])
plot(v(I),p(I),'r.','MarkerSize',20,'HandleVisibility','off');
end
figure(1);
title('I-V Characteristics')
plot(v(I),i(I),'r.','MarkerSize',20,'DisplayName','MPP');
legend(gca,'show','Location','Best')
xlabel('Output Voltage, V')
ylabel('Output Current, I')
axis([0 S*Voc 0 P*Isc])
grid on
figure(2);
title('P-V Characteristics')
plot(v(I),p(I),'r.','MarkerSize',20,'DisplayName','MPP');
legend(gca,'show','Location','Best')
xlabel('Output Voltage, V')
ylabel('Output Power, P')
axis([0 S*Voc 0 S*P*Pmax])
grid on
G=1000;
for (Temp=25:25:75)
sim('PVArray2')
v = V.signals.values;
i= I.signals.values;
p=v.*i;
[pmax,I] = max(p)
%legend_info = ['T=25^{\o}C, G=' num2str(c) 'W/m{^2}'];
```

```
figure(3);
hold all
plot (v,i,'DisplayName',['T=' num2str(Temp) '^{\o}C, G=' num2str(G) 'W/m{^2}'])
plot(v(I),i(I),'r.','MarkerSize',20,'HandleVisibility','off');
figure(4);
hold all
plot (v,p,'DisplayName',['T=' num2str(Temp) '^{\o}C, G=' num2str(G) 'W/m{^2}'])
plot(v(I),p(I),'r.','MarkerSize',20,'HandleVisibility','off');
end
figure(3);
title('I-V Characteristics')
plot(v(I),i(I),'r.','MarkerSize',20,'DisplayName','MPP');
legend(gca,'show','Location','Best')
xlabel('Output Voltage, V')
ylabel('Output Current, I')
axis([0 S*Voc 0 P*Isc])
grid on
figure(4);
title('P-V Characteristics')
plot(v(I),p(I),'r.','MarkerSize',20,'DisplayName','MPP');
legend(gca,'show','Location','Best')
xlabel('Output Voltage, V')
ylabel('Output Power, P')
axis([0 S*Voc 0 S*P*Pmax])
grid on
clear all
```

A.2   MPPT controller code

```
function D2  = PO(D_i,D_max,D_min,dD, V2, I2)
persistent V1 P1 D1;
if isempty(V1)
V1=0;
P1=0;
D1=D_i;
end
P2= V2*I2;
dV= V2 - V1;
dP= P2 - P1;
if abs(dP) >= .3
   if dP < 0
      if dV < 0
      D2= D1 - dD;
      else
      D2 = D1 + dD;
      end
      else
      if dV < 0
      D2 = D1 + dD;
      else
      D2 = D1 - dD;
      end
```

```
    end
    else D2=D1;
    end
    if D2 >= D_max || D2<= D_min
    D2=D1;
end
D1=D2;
V1=V2;
P1=P2;
```

A.3 Boost Converter Design

```
Ns=15;
Np=2;
fs=10e3;
ts=1/fs;
Pm=Ns*Np*200.143 %max Power
Vm=Ns*26.3 %V at max power
Vo=700;
Im=Pm/Vm;
r=.02;
D=1-Vm/Vo;
Io=Pm/Vo
Ro=Vo/Io
C_boost=ts/Ro/r % D=1
L_boost=100*Vo*ts/16/Io  %D=.5
```

A.4 Filter Design

```
clc
%Step1-----Calculate Zb,Lb,Cb
%Inputs
VLL =   400;     % line to line rms voltage
Vph =   400/sqrt(3);      % phase rms voltage
Pn  =  6e3;       % rated active power (Pmpp at STC)
Vdc =   700;      % dc-link voltage
fg =    50;     % gride frequncy
fsw_i = 25e3;      % inverter switching frequncy

%Step2-----Calculate Zb,Lb,Cb
Vb=VLL;
Pb=Pn;
Ib=Pn/(sqrt(3)*VLL);
Zb=VLL^2/Pn;
Lb=Zb/(2*pi*fg);
Cb=1/(2*pi*fg*Zb);

%Step3-----Calculate Cf (maximum power factor variation seen by  the grid is less than
5%)
x=2.5/100;
Cf=x*Cb;
```

%Step4-----Calculate Li (deltaIb=Vdc/(8*fsw_i*Li))deltaIb between 10-25%
deltaIb=.1*Ib;   %(10% * Imax)
Li=Vdc/(8*fsw_i*deltaIb)

%Step5-----Calculate Lg
Af = 20/100; %attinuation factor is 20% , maximum ripple= (20/100)*(10/100)=2%
Lg=(Af+1)/(Af*Cf*(2*pi*fsw_i)^2)

%Step6-----test Lf<.1pu
Lf=Lg+Li;
Lfpu=Lf/Lb
Lfpu_tets=Lfpu<.1

%Step7-----Calculte fres
Wr=sqrt((Li+Lg)/(Li*Lg*Cf));
fres=Wr/(2*pi); % resonance frequncy

%Step7-----make sure that 10f1<(fres)<fsw/2
fres_Test=(fres>10*fg) && (fres<fsw_i/2)

%Step8-----Calculate Rf (damping resistor)
Rf= 1/(3*2*pi*fres*Cf)
%Rf=0

%step9 transfer function
num= [Cf*Rf 1];
den=[Li*Lg*Cf (Li+Lg)*Cf*Rf (Li+Lg) 0];
G1=tf(num,den)

bode(G1),grid